measurement systems laboratory

massachusetts institute of technology, cambridge, massachusetts 02139

TE-48

**RIDE COMFORT CONTROL IN
LARGE FLEXIBLE AIRCRAFT**

by

Michael Edward Warren

JAN 1972
RECEIVED

NASA CR 116775

TE-48

RIDE COMFORT CONTROL IN LARGE FLEXIBLE AIRCRAFT

by

MICHAEL EDWARD WARREN

APPROVED: _____ W. Markey _____
                    Director
                    Measurement Systems Laboratory

RIDE COMFORT CONTROL IN LARGE FLEXIBLE AIRCRAFT

by

MICHAEL EDWARD WARREN

S.B., Massachusetts Institute of Technology (1969)

SUBMITTED IN PARTIAL FULFILLMENT

OF THE REQUIREMENTS FOR THE

DEGREE OF MASTER OF SCIENCE

at the

MASSACHUSETTS INSTITUTE OF TECHNOLOGY

Signature of Author_____
                         Department of Aeronautics and Astronautics
                                      May 1971

Certified by _____
                                                Thesis Supervisor

Accepted by_____
               Chairman, Departmental Committee on Graduate Students

RIDE COMFORT CONTROL IN LARGE FLEXIBLE AIRCRAFT

by

Michael Edward Warren

Submitted to the Department of Aeronautics and Astronautics on May 14, 1971 in partial fulfillment of the requirements for the Degree of Master of Science.

ABSTRACT

The problem of ameliorating the discomfort of passengers on a large air transport subject to flight disturbances is examined. The longitudinal dynamics of the aircraft, including effects of body flexing, are developed in terms of linear, constant coefficient differential equations in state variables. A cost functional, penalizing the rigid body displacements and flexure accelerations over the surface of the aircraft is formulated as a quadratic form. The resulting control problem, to minimize the cost subject to the state equation constraints, is of a class whose solutions are well known. The feedback gains for the optimal controller are calculated digitally, and the resulting autopilot is simulated on an analog computer and its performance evaluated.

Thesis Supervisor: John J. Deyst, Jr.
Title: Assistant Professor of
                  Aeronautics and
                  Astronautics

ACKNOWLEDGMENTS

CONTENTS

Page

INTRODUCTION

The design of an autopilot system to improve the ride quality of
transport aircraft is a formidable task. The system commonly accepts
data from a number of sensors placed at various points throughout
the airframe, and outputs command signals to the aircraft control sur-
faces. The autopilot designer must synthesize this multi-input/output
system and evaluate the performance of the design in terms of the ride
quality at all seats of the airplane. Conventional methods of control
system design (Bode, Root Locus, etc.) readily handle questions on
stability and transient response, but are generally insufficient to
provide the subtle insights necessary to determine how gain ratios or
feedback paths should be altered to improve the overall ride quality.
In the work presented here, it will be shown that this autopilot
design problem can be formulated realistically as an optimal control
problem. A solution will be demonstrated for a typical supersonic
transport aircraft and the resulting design evaluated by simulation
on an analog computer.

The first attempt at development of a ride quality autopilot was
the result of flight test experience with the XB-70 experimental bomber,
where high sensitivity to input gusts in the forward fuselage area
resulted in an uncomfortable acceleration environment for the crew.
(This problem has since been lessened by the implementation of the
ILAF control system on the XB-70). While this situation remains
undesirable in a military aircraft, it is intolerable in a civilian
transport, where the concept of ride quality becomes exceedingly
important.

Aircraft flexing is only one detractor from passenger ride comfort.
The characteristic vertical motion of the airplane, resulting from

excitation of the short period mode, adds to rider discomfort. While the total displacements due to airframe flexure may be small, typically the accelerations due to the flexing occur at frequencies which are most annoying to human subjects. On the other hand, the large vertical motion of the aircraft, while not contributing significantly to the disturbing accelerations, may cause dizziness or motion sickness. Any attempt to control the ride quality of an airplane must consider these two differing contributors.

The Boeing swept-wing SST Transport prototype (B-2707) was chosen as a model for this investigation. As a proposed civilian airliner, ride comfort is important, and the design is such to induce greater fuselage flexibility than in previous commercial airplanes, and even the XB-70. It should be pointed out, however, that unlike the XB-70, the B-2707 flexure modes are well behaved in that flexure disturbances are not concentrated in either forward or aft fuselage sections.

As the attempt of this thesis is to investigate the control problem associated with minimizing ride discomfort of a large flexible aircraft, rather than to design a particular control system for a particular airplane, an idealized and simplified mathematical model of the B-2707 was chosen. The dimensions of the model are almost identical to those of the B-2707, however, the mass distribution of the model was assumed constant over the fuselage and constant over the lifting surfaces. This two phase distribution allowed for the mass and center of gravity of the model to be consistent with those of the B-2707. The effective deviation from the actual aircraft is most probably small (whenever the mass distribution arises, it is smoothed via integration), yet the freedom from following minute detail of the aircraft allows for more insight into the structure of the problem at hand. The idealized model is shown in Figure 1. Numerical values

relating to physical aspects of the model were either given in the Boeing 2707 Airframe Design Report (Ref. 2), or else were derived to conform to some expected behavioral characteristic of the B-2707. In either case, the origin of numerical data will be made clear as they arise in the text.

Before one can tackle the problem of flexure control with the expectation of manageable results, vast simplifications must be achieved. The problem is of a distributed nature; the vibrating structure has an infinity of natural modes. The complex dynamic interactions of subassemblies, wings, fuselage, engine nacelles, as well as concomitant forms of flexing, tortional vs. longitudinal, complicate the problem to extraordinary degree. Evidently, it would be advantageous to effect both a decoupling between flexing of subassemblies and an approximation of the distributed system by a finite number of modes.

In the succeeding chapter, a model for the flexure dynamics of the idealized aircraft will be developed. The particular model will obviously depend critically upon the elastic and inertial properties of the structure. The flexure analysis in this paper ignores the effect of aerodynamics upon the elastic properties of the vehicle. The result is a model in which the airplane vibrates according to a set of uncoupled modes. If the local changes in aerodynamic loading due to aircraft flexure were included, then the forcing terms, for example, would no longer be independent of the motion of the aircraft, and the resulting equations of vibration would become inexorably coupled. However, as the displacements of the elastic structure due to flexing are small, the deviations from nominal aerodynamic forces will be correspondingly small.

F = fuselage

W = wing

T = tail

E = elevator
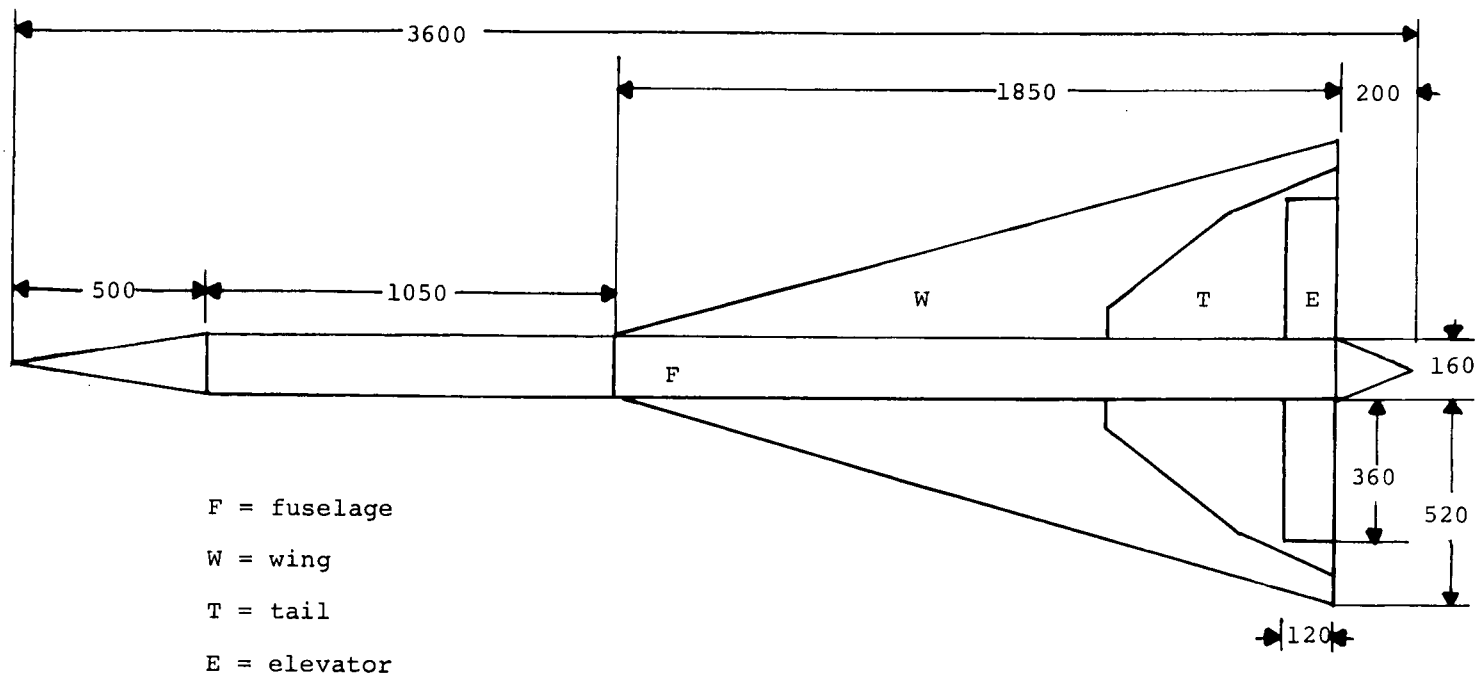
Figure 1. Idealized SST Model (all dimensions in inches)

It should be understood that large differences in the flight condition may change the nominal aerodynamic loading on the aircraft structures greatly. Thus, the model derived in this investigation, based on conditions of constant speed, constant altitude, steady state flight may be inappropriate for other flight conditions, such as steep climbing.

Control surfaces available to the controller will consist solely of the elevators.* In the swept wing supersonic phase of flight, the elevators represent the major normal force producing control surfaces. They are generally effective in producing pitching moments and in tailess aircraft, (In the sweptback wing configuration, the B-2707 is essentially a tailess aircraft.) adept also in producing left. In addition, the position of the elevators does not coincide with any nodes of the flexing motion, hence forces applied through the elevators will influence all the deflection modes.

---

*Although only the elevators are considered in this development, other control effectors (flaps, spoiler, etc.) could be readily included.

CHAPTER 1

The Physical Problem

In this chapter, a model of the airplane will be developed suitable for a control formulation of the problem. Section A will explore the flexure dynamics of the idealized aircraft. The problem of rigid body motion and the aerodynamic properties involved are discussed in Section B. Control elements and control forces are examined in Section C and a suitable cost functional is developed in Section D. In addition, supplemental information and detailed calculations have been inserted as appendices and are referenced throughout the chapter.

A. Flexure Dynamics

A.1. Introduction

Although the modal response of an elastic airframe is a distributed parameter system, intuitive considerations demand that the response at higher frequencies become vanishingly small lest a bounded energy input give rise to an unbounded energy output. An in depth analysis of the B-2707 confirms this and suggests that only the first five vibration modes can be considered at all significant. (Ref. 2, p.52) Further data shows that although the frequency response of the airplane to inputs at the fifth modal frequency (5.09 cps) is not insignificant, the harmonic content of realistic atmosphere gust models is appreciably lower. Hence in flight conditions subject to random gust disturbances, the excitation of the fifth mode is minimal, and it suffices to examine just the first four modes. The natural vibration characteristics corresponding to these modes are shown in Figure 2. and refer to the lightweight (375,000 lb.) configuration of the airplane.

It is instructive to examine closely the natural modes, for

their particular shapes shed much light on the modeling problem. From Figure 2, certain modal characteristics stand out. The first and fourth modes (1.47 and 3.81 cps, respectively) consist mainly of fuselage flexing and tend to be sinusoidal in shape. The wing and tail act to limit the motion of the aft section of the fuselage in the first mode, as these lifting surfaces vibrate in tandem. In the fourth mode however, the lifting surface motion is seen to be of a scissoring nature, and while still introducing damping into the vibrating system, has a minimal effect on the range of motion exhibited by the rear sections of the passenger compartment. The second mode (2.25 cps) consists almost entirely of lifting surface motion. Here again, the wing and tail scissor, inducing scarcely any motion along the fuselage. Mode three (2.56 cps) is again primarily lifting surface flexure, but in this case, wing and tail motion is in tandem, and the effect is greater fuselage flexing than in the former case.

Judging from Figure 2 and the preceeding discussion, the decomposition of the airframe into independent flexing subassemblies would seem at first glance a profitable avenue of attack. Through a proper decomposition, it should be possible to model the subassemblies with a degree of homogeneity lacking in the entire aircraft. For example, we might want to divorce the wings from the fuselage in our model, considering each as an independent structure, and superpositioning solutions with appropriate boundary conditions. Whatever the decomposition, we would demand that the autonomously derived solutions adequately conform to the expected mode shapes in Figure 2.

Therein is where the problem lies. The boundary conditions which need to be matched up when the components are reassembled are time varying. Whatever simplifications occur by the decomposition are more
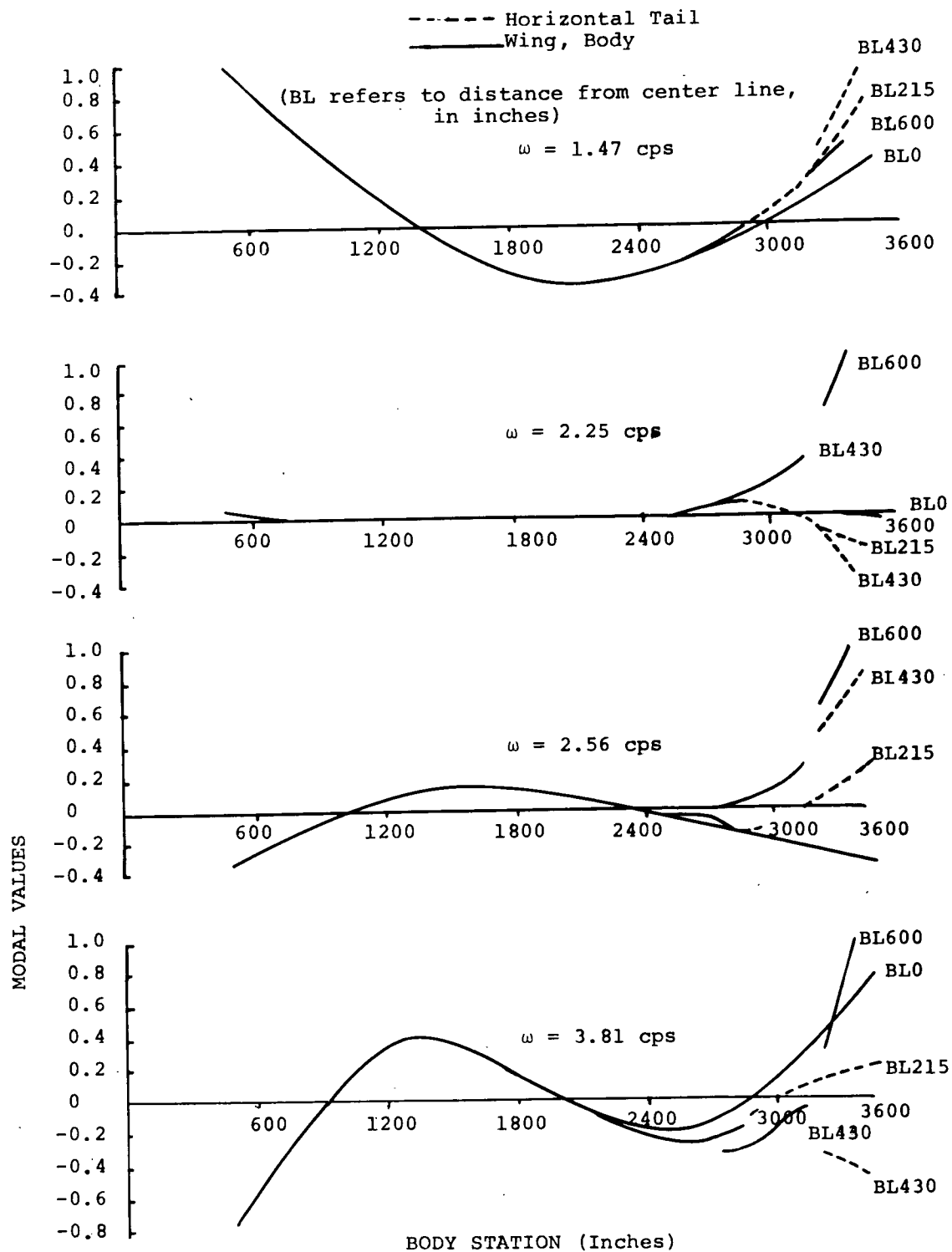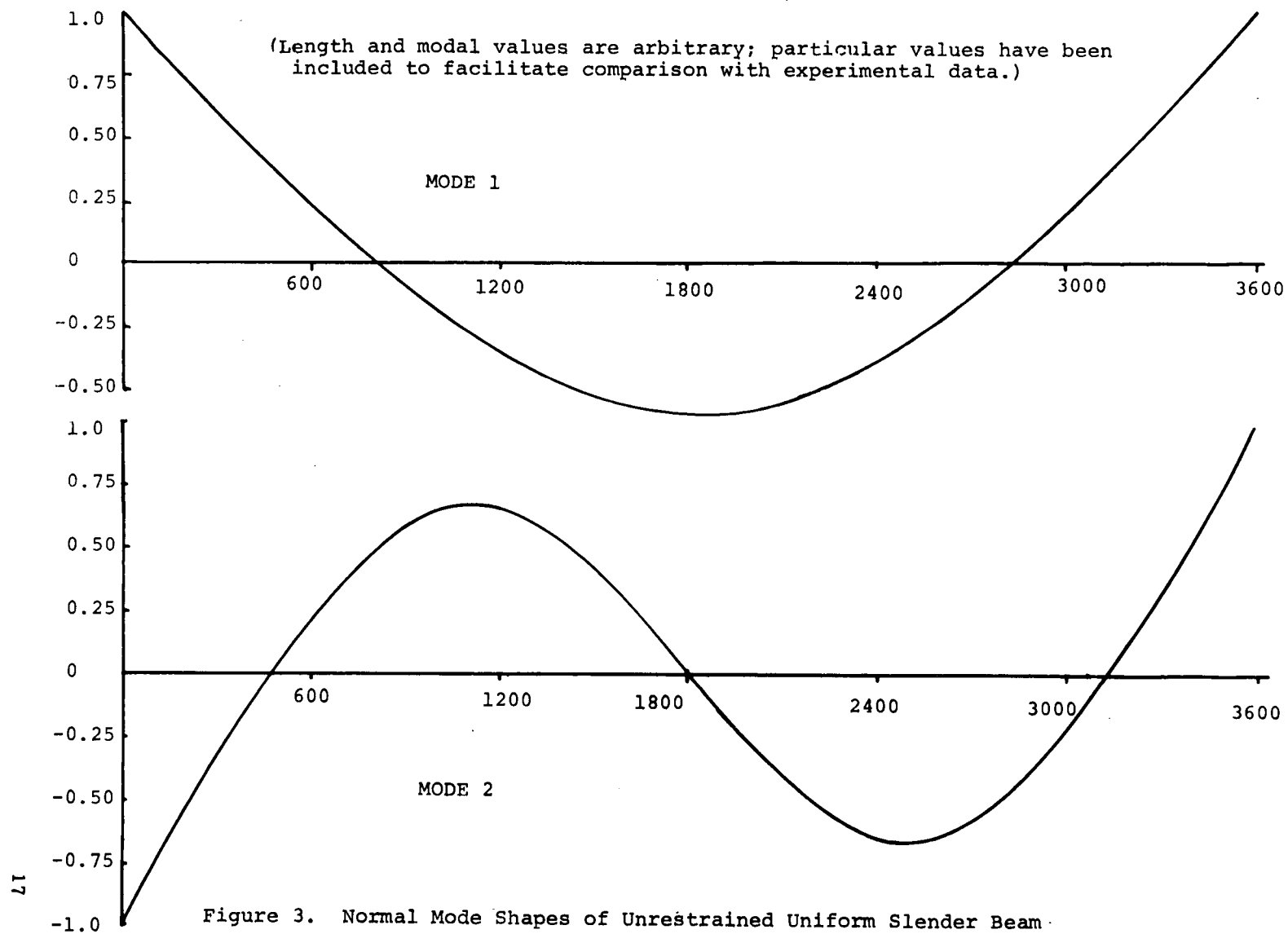
14

Figure 2. Natural Vibration Characteristics, B-2707

than counterbalanced by the complications of the boundary conditions. Yet the idea is not a totally fruitless endeavor. The investigation of the flexure of the independent subassemblies, if not yielding closed form solutions, nevertheless sheds much light on the dominant motions of the flexing aircraft. Even more important, the theory of long, slender elastic beams which is often brought into play to model the various airframe components, extends quite naturally to problems of elastic plates. It is the theory of elastic plates which will allow us a framework for a simple, yet highly applicable model for airframe flexure.

For the reasons outlined above, we will take a small digression and examine briefly the flexure dynamics of the dominant subassembly, the fuselage. Any model of the fuselage dynamics must satisfactorily account for the first and fourth flexing modes of Figure 2, as these are seen to be composed primarily of fuselage vibrations. A seemingly reasonable and yet simple choice would be to equate the fuselage to a long slender beam of appropriate mass distribution and stiffness. Disregarding the extreme forward and aft fuselage sections, there is little reason to expect anything other than a fairly uniform mass distribution along the length of the fuselage. This model yields mode shapes (Figure 3) which are very similar to the manufacturer's vibration characteristics, modes one and four. In addition, the beam theory predicts a ratio of 2.77 between the first two normal mode frequencies. The manufacturer's data on the B-2707 has shown the two fuselage dominant modes to be separated by a factor of 2.56, in close accord with the uniform beam theory.

The application of the beam theory provides us with a model which is well understood, and soluble. As the rotary inertia and transverse shear deformations of the airplane fuselage are negligible in the

16

(Length and modal values are arbitrary; particular values have been included to facilitate comparison with experimental data.)

MODE 1

MODE 2

Figure 3. Normal Mode Shapes of Unrestrained Uniform Slender Beam

17

assumed flight configuration, these terms may be omitted in the beam
model, yielding a solution which can be exhibited in closed form.
Appendix A, Sections 1 and 2, contain derivations of both the differential
and integral equations of motion for the slender beam. Both analyses
are included as they represent different mathematical approaches
to the same problem, and tend to complement each other. The reader
should note the inherent similarities in the derivations of the inte-
gral equations of motion for the simple beam and the unrestrained
aircraft. The latter is given in Appendix 1, Section 3.

A.2 Free Vibration of the Unrestrained Airplane

The two dimensional theory derives its impetus from the simple
beam analysis. It assumes that a three dimensional aircraft is com-
pressed into a flat elastic plate, rigid in its own plane and able
to execute small displacements in vertical position, pitch and roll in
addition to elastic motion. Although these assumptions do involve a
loss of generality, they allow us to draw upon previously established
beam theory in developing a simple yet adequate model for aircraft
aeroelasticity.

Consider an airplane idealized as an elastic plate and a super-
imposed coordinate system, so that the aircraft is in the x-y plane,
with the x-axis along the length of the fuselage. Furthermore, the
coordinate axes coincide with the principal inertial axes of the air-
plane and the origin of the system is at the center of gravity of the
vehicle. As the structure is vibrating freely, the coordinate axes
may be considered fixed in space.

Let us denote the displacement of the elastic surface along the
z-axis by $w(x,y,t)$. Then in the absence of external forces, moment

18

equilibrium about the x and y axes together with force equilibrium demand that:

$$\iint_S \ddot{w}(x,y,t)\rho(x,y)dxdy = 0 \qquad (1-1)$$

$$\iint_S \ddot{w}(x,y,t)x\rho(x,y)dxdy = 0 \qquad (1-2)$$

$$\iint_S \ddot{w}(x,y,t)y\rho(x,y)dxdy = 0 \qquad (1-3)$$

where $\rho(x,y)$ represents the mass distribution over the surface of the airplane. Additionally, we obtain an equation relating the elastic and inertial forces

$$w(x,y,t) - w(0,0,t) - x\,\frac{\partial w(0,0,t)}{\partial x} - y\,\frac{\partial w(0,0,t)}{\partial y} \qquad (1-4)$$

$$= -\iint_S C(x,y;\xi,\eta)\rho(\xi,\eta)\ddot{w}(\xi,\eta,t)d\xi d\eta$$

where $C(x,y;\xi,\eta)$ is a two dimensional influence function, measuring the deflection at a point (x,y) due to a unit force applied at the point (ξ,η) when the origin of the x-y plane is clamped. Equation (1-4) is well motivated by the development of the integral equations of motion for a simple beam in Appendix A, Section 2.

The equations of motion for the elastic plate are separable, i.e. they admit a solution of the form

$$w(x,y,t) = W(x,y)T(t) \quad . \qquad (1-5)$$

Upon the introduction of (1-5) and some simplification, the equations can be rewritten in the form:

$$\ddot{T} + \omega^2 T = 0 \qquad\qquad (1-6)$$

$$W(x,y) = \omega^2 \iint_S G(x,y;\xi,\eta) W(\xi,\eta) \rho(\xi,\eta) d\xi d\eta \qquad\qquad (1-7)$$

where

$$G(x,y;\xi,\eta) = C(x,y;\xi,\eta) - \iint_S C(r,s;\xi,\eta) \left[\frac{1}{M} + \frac{xr}{I_y} + \frac{ys}{I_x}\right] \rho(r,s) drds. \quad (1-8)$$

Equation (1-8) defines the influence function of the unrestrained air-
craft. As in the case of the unrestrained beam, the integral term in
Eq. (1-8) has the effect of subtracting off the rigid body motion of
the aircraft. Equations (1-6) and (1-7) can be solved for a family
of solutions, each pair T_j and W_j corresponding to a particular value
of ω. The functions satisfying Eq. (1-7) are the natural mode shapes
of the system and represent the characteristic shapes of the distor-
tions of the elastic surface. The derivation of the equations of
free vibration are given in Appendix A, Section 3. In addition, the
mode shapes are orthogonal to each other with respect to the mass
distribution function $\rho(x,y)$:

$$\iint_S W_m W_n \rho dx dy = 0 \quad . \qquad\qquad (1-9)$$

This most important characteristic is proved in Appendix A, Section 4.

A.3 Forced Motion of the Unrestrained Aircraft

Before the problem of forced motion of the aircraft can be tackled,
it is necessary to redefine the meaning of the displacement function
$w(x,y,t)$. For the situation of free vibration, $w(x,y,t)$ represents

20

the displacement with respect to the airplane principal inertial axes, which may be assumed stationary in space. We are afforded the opportunity to measure the elastic motion alone by subtracting out the gross rigid body motion. Reference to Equation (1-7) will indicate that the rigid body mode shapes for the freely vibrating beam are indeed vacuous. For forced motion, it is no longer possible to pre-calculate and subtract the rigid body displacements, hence $w(x,y,t)$ must represent the total displacement of the elastic surface including gross translations and rotations.

As is customary when considering only longitudinal dynamics, we restrict our study to an elastic airframe free to pitch and plunge, but restrained against rolling. $F_z(x,y,t)$ will represent the applied force in the z-direction per unit surface area. By simple equilibrium of forces and moments we have:

$$\iint_S \ddot{w}(x,y,t)\,\rho(x,y)\,dxdy \;=\; \iint_S F_z(x,y,t)\,dxdy \tag{1-10}$$

$$\iint_S \ddot{w}(x,y,t)\,\rho(x,y)\,xdxdy \;=\; \iint_S F_z(x,y,t)\,xdxdy \,. \tag{1-11}$$

Analogous to Equation (1-4) the relation between inertial and elastic forces becomes

$$w(x,y,t) \;-\; w(0,0,t) \;-\; x\,\frac{\partial w(0,0,t)}{\partial x}$$

$$= \iint_S C(x,y;r,s)\,[F_z(r,s,t) \;-\; \ddot{w}(r,s,t)\,\rho(r,s)]\,drds \,. \tag{1-12}$$

As in the case of the simple beam [See Appendix A, Section 1 or 2]

we represent the solution to the equations above as an infinite sum
of normalized mode shapes and normal (or generalized) coordinates.

$$w(x,y,t) = \sum_{n=1}^{\infty} \phi_n(x,y)\xi_n(t) \tag{1-13}$$

The normalized mode shapes $\phi_j(x,y)$ are simply the natural mode
shapes given by the solution of Equation (1-7) multiplied by a parti-
cular constant. Different procedures for normalizing the mode shapes
are in wide use. The manufacturer's mode shapes in Figure 2 have
been scaled so that the maximum value is unity. Another method em-
ployed is

$$\phi_j = \left[\frac{M_1}{\iint_S w_j^2 dxdy} \right]^{1/2} w_j \quad . \tag{1-14}$$

The use of M_1, the aircraft total mass, above is arbitrary as any
characteristic of the aircraft may be used. The result of normaliza-
tion by Eq. (1-14) is that the integral over the surface of the squared
modal deflection weighted by the mass distribution is a constant. This
integral, the generalized mass, arises in the resultant equations of
motion. The actual normalization technique used is arbitrary, and in
fact every mode can have a different and independently derived multi-
plicative constant without effecting the resultant calculated motion.

As the displacement function $w(x,y,t)$ consists of the total
motion of the elastic airframe, one normal mode must illustrate the
translation of the center of gravity and another the pitching rotation
about the c.g. Thus we designate

$$\phi_1(x,y) = 1; \qquad \omega_1 = 0 \tag{1-15}$$

$$\phi_2(x,y) = x; \qquad \omega_2 = 0 \quad . \tag{1-16}$$

These two modes represent the motion of the x-y plane while the remaining modes signify elastic motion with respect to the x-y plane. Hence these elastic deformation modes are identical to those in the case of free vibration of the aircraft, and satisfy Equations (1-1), (1-2) and (1-4). With the family of normalized mode shapes, so specified, the equations of motion can be simplified to

$$M_n \ddot{\xi}_n + \omega_n^2 M_n \xi_n = Z_n \qquad n = 1,2... \qquad (1-17)$$

where

$$M_n = \iint_S \phi_n^2 \rho \, dxdy \qquad (1-18)$$

is the generalized mass of the nth mode and

$$Z_n = \iint_S F_z \phi_n \, dxdy \qquad (1-19)$$

is the generalized force of the nth mode.

As previously discussed, the particular values of M_n and Z_n depend upon the normalization scheme employed. For example, if Equation (1-14) were used then we would have $M_n \equiv M_1$ for all n. The method of normalization has no effect whatsoever on the calculated motion, for the product $\phi_N \xi_N$ is independent of the particular scaling value used to fix ϕ_n. This is easily seen from Equation (1-17) together with the definitions of generalized mass and the generalized force.

A further note on the simplifications in the previous analysis is due. The free aircraft mode shapes derived from Equation (1-7) are slightly different than the manufacturer's mode shape data for a specific flight condition, such as those presented in Figure 2. This is because the modal excitations will produce small changes in local

angle of attack producing velocity dependent aerodynamic damping terms. The net effect of these terms is to change slightly the natural mode shapes and natural frequencies of the airplane. Similarly, the equations governing the normal coordinates (1-17) ignore structural damping effects. These terms are generally accounted for by the introduction of a small constant damping term (0.01 to 0.03) in the differential equations for ξ_i. It should be clear that the introduction of these additional effects may couple the modes of the unrestrained aircraft.

B. Rigid Body Motion

The preceding analysis of the forced motion of the elastic air-frame leads directly to equations governing the pitching and plunging motion of the aircraft, (A.5-11) and (A.5-10) respectively. However, these equations are derived without consideration of aerodynamic effects, which although negligible for small elastic deformations, may be significant for larger rigid body motions. Hence it would seem beneficial to derive expressions for the rigid body motion of the airplane incorporating the aerodynamic forces acting on the structure. It should be clearly understood that a reformulation of the equations governing the rigid body motion will not affect the validity of Equation (1-17), governing the elastic deformations. The derivation of Eq. (1-17) is in no way dependent upon the particular time functions for translation and rotation, $\xi_1(t)$, and $\xi_2(t)$, [See Appendix A, Section 5], but rather upon the mode shapes for these motions, which remain unchanged.

The rigid body motion is most easily examined by a small pertur-bation analysis about a level equilibrium flight condition. The resulting ordinary differential equations are not cumbersome, and

24

are quite adequate when the deviations from nominal flight conditions are small. We are concerned with the pitching and plunging motion of the aircraft described by the following set of equations:

$$\frac{mU_0}{qS} \frac{\dot{u}}{U_0} - C_{x_u} \frac{u}{U_0} - C_{x_\alpha} \alpha + \frac{mg}{qS} \theta = 0 \qquad (1\text{-}20)$$

$$-C_{z_u} \frac{u}{U_0} + \frac{mU_0}{qS} \dot{\alpha} - C_{z_\alpha} \alpha - \frac{mU_0}{qS} \dot{\theta} - C_{z_\rho} \frac{h}{h_0} = C_{z_\delta} \delta \qquad (1\text{-}21)$$

$$-C_{m_u} \frac{u}{U_0} - \frac{c}{2U_0} C_{m_{\dot{\alpha}}} \dot{\alpha} - C_{m_\alpha} \alpha + \frac{I_y}{qSc} \ddot{\theta} - \frac{c}{2U_0} C_{m_{\dot{\theta}}} \dot{\theta} = C_{m_\delta} \delta \qquad (1\text{-}22)$$

$$\frac{U_0}{h_0} \alpha - \frac{U_0}{h_0} \theta + \frac{\dot{h}}{h_0} = 0 \qquad (1\text{-}23)$$

where the perturbation quantities are: u, velocity; α, angle of attack; θ, pitch angle; h, altitude; and δ, elevator deflection. The equations (1-20) through (1-23) are examined and put in the form of a minimum realization linear system in Appendix B. The interested reader is directed to Reference 5 for a complete derivation and a more exhaustive study.

The effect of the rigid body dynamics is to superimpose an oscillatory motion on the constant altitude nominal flight trajectory. This motion, the short period mode of the airplane is characterized by a low frequency sinusoidal impulse response in angle of attack and pitch rate perturbations. The center of gravity location is most important in the short period mode response as it determines the aerodynamic restoring moments due to a perturbation in angle of attack. The further forward the center of gravity, the larger the restoring moments.

Approximate dynamics for this motion are obtained by examining the homogeneous response of the dominant second order system in angle of attack and pitch rate perturbations:

$$\frac{mU_0}{qS} \dot{\alpha} - C_{z_\alpha} \alpha - \frac{mU_0}{qS} \dot{\theta} = 0 \qquad\qquad (1\text{-}24)$$

$$- \frac{c}{2U_0} C_{m_{\dot{\alpha}}} \dot{\alpha} - C_{m_\alpha} \alpha + \frac{I_y}{qSc} \ddot{\theta} - \frac{c}{2U_0} C_{m_{\dot{\theta}}} \dot{\theta} = 0 \qquad . \qquad (1\text{-}25)$$

Disregarding the $C_{m_{\dot{\alpha}}}$ term as it is most often negligible, the characteristic equation for this motion is easily shown to be

$$\lambda^2 + 2d\omega_n \lambda + \omega_n^2 = 0 \qquad\qquad (1\text{-}26)$$

where

$$\omega_n^2 = \frac{C_{z_\alpha} C_{m_{\dot{\theta}}} \frac{c}{2U_0}}{\frac{mU_0}{qS} \frac{I_y}{qSc}} - \frac{C_{m_\alpha}}{\frac{I_y}{qSc}} \qquad\qquad (1\text{-}27)$$

and

$$2d\omega_n = - \left[\frac{C_{z_\alpha}}{\frac{mU_0}{qS}} + \frac{\frac{c}{2U_0} C_{m_{\dot{\theta}}}}{\frac{I_y}{qSc}} \right] . \qquad\qquad (1\text{-}28)$$

In the SST model, the center of gravity is quite far aft and the wing loading is light, resulting in small restoring moments and a relatively long period for the rigid body motion. The approximate values for natural frequency, ω_n, and damping ratio, d, are calculated to be 1.48 sec^{-1} and 0.177 respectively.

C. The Control

For this investigation, the control surfaces will be restricted to the elevators. In the swept wing B-2707 the elevators represent

26

the major control surfaces with which the pilot can vary forces in the z-direction. As would be expected, elevator deflections are an efficient means of producing rigid body motion of the aircraft, particularly pitching moments. Furthermore, as the elevators do not coincide with the nodes of any significant elastic deformation modes, these control surfaces should be effective in both stimulating and controlling aircraft flexure.

In the sweptwing configuration, the wing and tail form one continuous lifting surface. (See Figure 1). If the elevator deflection is non-zero, i.e. the elevator and the wing surface intersect at a non-zero angle, then the elevator acts as a new lifting surface with an angle of attack equal to the elevator deflection, measured downward as positive. From elementary supersonic flow theory, the coefficient of lift of a flat plate at an angle of attack α is

$$C_L = 4\alpha (M_0^2 - 1)^{-1/2} \tag{1-29}$$

where M_0 is the Mach number. Hence the normal force per unit area of the elevator, per unit elevator deflection is given by

$$F_z = 4(M_0^2 - 1)^{-1/2} q \tag{1-30}$$

where q is the dynamic pressure (one half the atmospheric density times the square of the aircraft velocity).

D. The Cost Criterion

As mentioned in the introduction, the control objective of this study is to minimize the passenger discomfort associated with the rigid body and flexing motion of the airplane due to wind gusts. This discomfort arises from two quarters. First there is the effect of

undesirable accelerations of the aircraft structure yielding a rough ride. Second is the low frequency roller-coaster type of motion which even without significant accompanying acceleration, can provide a most unpleasant flight experience. The discomfort is the result of a number of factors including the pitch motion of the aircraft, changes in sound level of the engines and low level vertical accelerations, all occuring at the same low frequency. Although it is difficult to assess all of these factors, an overall measure of discomfort is the magnitude of changes in altitude that result from the roller coaster type motion.

Studies of human vibration response have shown that human discomfort varies not only with the magnitude of disturbing accelerations, but with their frequency as well. People seem to have an extreme distaste for accelerations applied at frequencies between four and eight cycles per second. This particular phenomenon is graphically shown in Figure 4, which represents tests conducted in concert with SST flexure studies.

Figure 4 suggests that passengers riding the SST would be fairly sensitive to the accelerations induced by the aircraft flexure, occurring at frequencies from 1.47 to 3.81 cps. We might then expect if the gross motion due to flexure were small enough, that the primary influence of the flexure modes on the ride comfort is the acceleration environment of the passenger compartment. This is exactly the situation that has occurred in flight simulations. Although the elastic motions were considerably larger than for subsonic airliners, they were still small enough so that the acceleration environment was the predominant factor. [Ref. 2, p. 84] From Figure 4, we see that the low frequency rigid body accelerations (the dominant rigid body frequency is 0.232 cps) need to be quite large compared with the flexure accelerations before they exhibit the same degree of unpleasantness. However, the gross vertical motion of the airframe due to pitching and plunging may be orders of magnitude larger than the elastic motion. Thus it is
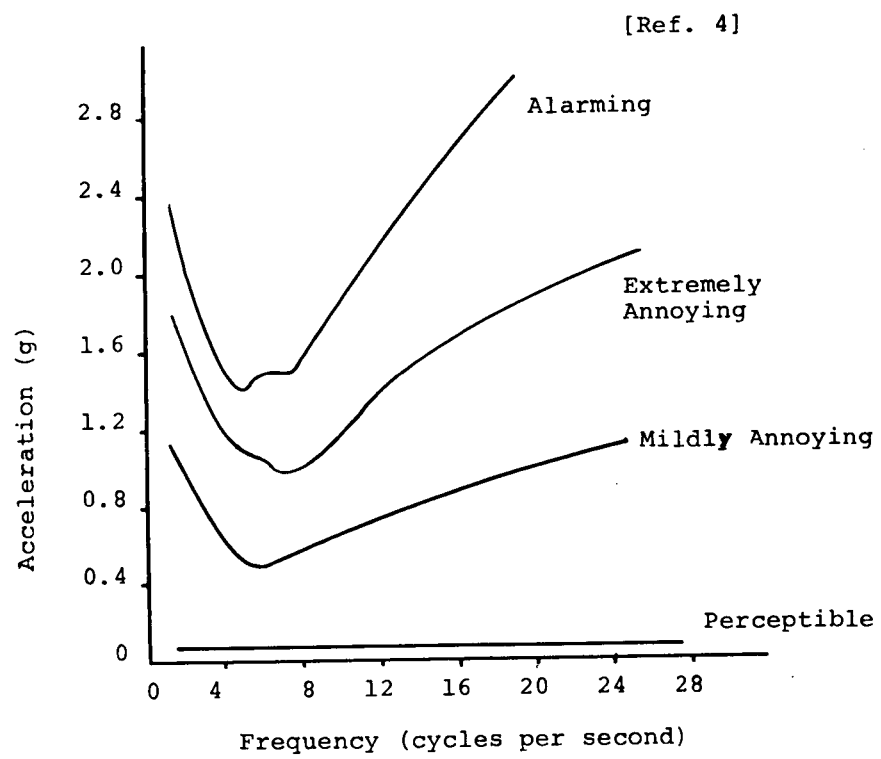
Figure 4. Subjective Human Vibration Response Curves (Medians)

likely that except for conditions of high turbulence, (which in general will occur at lower altitudes) the vertical motion due to the rigid body dynamics rather than the rigid body accelerations will have the predominant effect on passenger discomfort.

A reasonable control objective would thus be to minimize the square acceleration caused by the airplane flexure and the square perturbation in altitude caused by the rigid body motion over the duration of cruise. The critical independence of the response modes of the unrestrained airplane allows us to decouple the total motion of the aircraft, and weight separately characteristics of the disturbing behavior. The orthogonality of mode shapes will lead to considerable simplification of the functional representation of the control objective.

Let us deal first with the accelerations effected by the airplane flexure modes. From equation (1-17) we have

$$\ddot{\xi}_n = -\omega_n^2 \, \xi_n + \frac{1}{M_n} \iint_S F_z \phi_n dx dy \; . \tag{1-31}$$

From Section C we know that the normal force is restricted to the elevator and is proportional to the elevator deflection. Hence, in light of Eq. (1-30) we can write

$$\ddot{\xi}_n = -\omega_n^2 \xi_n + (G_n/M_n) \, \delta \tag{1-32}$$

where

$$G_n = \iint_E 4(M_0^2 - 1)^{-1/2} q \phi_n (x,y) dx dy \tag{1-33}$$

and the integration is restricted to the surface of the elevator. Multiplying Equation (1-32) by ϕ_n and then summing over the deformation modes (n = 3,4,...) yields the total acceleration due to flexure dynamics:

$$\ddot{w}_F(x,y,t) = \sum_{n=3}^{\infty} \phi_n(x,y) \, [-\omega_n^2 \xi_n(t) + \frac{G_n}{M_n} \delta]. \qquad (1-34)$$

As the acceleration of the fuselage is of greater import than the accelerations of the lifting surfaces, we would like to weight the fuselage more heavily than the wings and tail when integrating the squared acceleration function over the surface of the airplane. While arbitrary weighting functions may allow considerable latitude in the formulation of the cost functional, one particular function affords considerable simplification in the form of cost. As the mode shapes are orthogonal with respect to the mass distribution $\rho(x,y)$ [See Appendix A, Section 4] use of this as a weighting function will mean the absence of cross products of modes in the cost functional. In addition, for the idealized SST model, the mass distribution is significantly higher over the fuselage than for the lifting surfaces, and thus readily satisfies the original condition of a priority weighting. Accelerations of large mass elements are thus heavily penalized by this weighting scheme. It is reasonable to expect that the resulting control system will not allow large accelerations of massive structural subassemblies and hence will not produce excessive structural loading to achieve ride quality.

From Equation (1-34), we have the "cost" of the disturbing flexure induced accelerations, where T is the length of the cruise, as

$$\int_0^T \!\!\int\!\!\int_S \ddot{w}_F^2 \rho \, dx\,dy\,dt = \int_0^T \!\!\int\!\!\int_S \left[\sum_n \phi_n(-\omega_n^2 \xi_n + \frac{G_n}{M_n}\delta) \right]^2 \rho \, dx\,dy\,dt. \quad (1-35)$$

Let us denote the left hand side of Equation (1-35) by J_F. Expanding the bracketed term in the equation and making use of the orthogonality of the mode shapes we can write

$$J_F = \int_0^T \sum_n \iint_S \phi_n^2 \rho \, dxdy [\omega_n^4 \xi_n^2 - 2\omega_n^2 \frac{G_n}{M_n} \xi_n \delta + (\frac{G_n}{M_n})^2 \delta^2] dt \qquad (1\text{-}36)$$

which simplifies to

$$J_F = \int_0^T \sum_n M_n [\omega_n^4 \xi_n^2 - 2\omega_n^2 \frac{G_n}{M_n} \xi_n \delta + (\frac{G_n}{M_n})^2 \delta^2] dt \quad . \qquad (1\text{-}37)$$

For the rigid body modes, although we want to minimize vertical motion rather than accelerations, the approach is quite similar. The gross rigid body motion is given by

$$w_R(x,y,t) = h + x\theta \cdot \qquad (1\text{-}38)$$

Squaring w_R, weighting by the mass distribution and integrating over the surface of the airplane and the duration of the flight yields

$$\int_0^T \iint_S w_R^2 \rho \, dxdydt = \int_0^T \iint_S (h^2 + 2xh\theta + x^2\theta^2)\rho(x,y) dxdydt \quad (1\text{-}39)$$

Letting J_R denote the left hand side of (1-39), we can expand the integral on the right to obtain simply

$$J_R = M_1 \int_0^T h^2 dt + M_2 \int_0^T \theta^2 dt \quad . \qquad (1\text{-}40)$$

The entire cost for input disturbances then becomes

$$J = c_F J_F + c_R J_R \qquad (1\text{-}41)$$

where the weighting coefficients c_F and c_R can be adjusted to obtain any balance of control effort between flexing and rigid body motions.

The reader should notice that although the cost functional for the fuselage accelerations, Equation (1-37), does not include the damping terms mentioned in Section A.3, there is no difficulty in extending the cost to include this feature. Thus, if we add to the right side of Eq. (1-32) a term representing damping, $-2d_n \omega_n \dot{\xi}_n$, where d_n stands for the damping ratio of the nth mode, J_F becomes

$$J_F = \int_0^T \sum_n M_n [\omega_n^4 \xi_n^2 + 4d_n \omega_n^3 \xi_n \dot{\xi}_n + 4d_n^2 \omega_n^2 \dot{\xi}_n^2 - 2\omega_n^2 \frac{G_n}{M_n} \xi_n \delta$$

$$- 4d_n \omega_n \frac{G_n}{M_n} \dot{\xi}_n \delta + (\frac{G_n}{M_n})^2 \delta^2] dt \quad . \qquad (1-42)$$

CHAPTER 2

The Control Problem

This chapter of the thesis deals with the formulation, solution and implementation of the mathematical control problem motivated by the analysis of Chapter One. Section A presents the framework and solution of the problem. The computer implementation is considered in Section B. As in the preceeding chapter, detailed calculations have been relegated to the appendices.

A. Solution of the Control Problem

From the modeling of the physical system in Chapter 1, it is clear that the dynamics of the rigid body motion and the first four elastic modes can be combined in the framework of linear ordinary differential equations. Let us define the thirteen (13) component state vector $\underline{x}$ as follows:

$$\underline{x}' = [u \ \alpha \ \theta \ \dot{\theta} \ h \ \xi_3 \ \dot{\xi}_3 \ \xi_4 \ \dot{\xi}_4 \ \xi_5 \ \dot{\xi}_5 \ \xi_6 \ \dot{\xi}_6 \ ] . \qquad (2-1)$$

(To avoid confusion between vectors, matrices and scalars, the notation of lower case underlined letters for vectors, upper case underlined letters for matrices will be used. Scalars will not be underlined. The prime superscript on vectors or matrices denotes transpose.)
Note that $\underline{x}(t)$ is a differentiable function of time as are all its components.

We will define the matrix $\underline{A}$ as below:

$$
\underline{A} = \begin{bmatrix}
\underline{A}_1 & \underline{0} & \underline{0} & \underline{0} & \underline{0} \\[12pt]
\underline{0} & \underline{A}_3 & \underline{0} & \underline{0} & \underline{0} \\[12pt]
\underline{0} & \underline{0} & \underline{A}_4 & \underline{0} & \underline{0} \\[12pt]
\underline{0} & \underline{0} & \underline{0} & \underline{A}_5 & \underline{0} \\[12pt]
\underline{0} & \underline{0} & \underline{0} & \underline{0} & \underline{A}_6
\end{bmatrix} \tag{2-2}
$$

where $\underline{A}_1$, the system matrix of the rigid body motion, is given by [See Appendix B]

$$
\underline{A}_1 = \begin{bmatrix}
C_{x_u}/a & C_{x_\alpha}U_0/a \\[10pt]
C_{z_u}/a & C_{z_\alpha}/a \\[10pt]
0 & 0 \\[10pt]
b\left(\dfrac{C_{m_u}}{U_0} + \dfrac{c}{2U_0}\,C_{m_{\dot\alpha}}\dfrac{C_{z_u}}{U_0}/a\right) & b\left(-C_{m_\alpha} + \dfrac{c}{2U_0}\,C_{m_{\dot\alpha}}C_{z_\alpha}/a\right) \\[10pt]
0 & -U_0
\end{bmatrix}
$$

$$
\begin{bmatrix}
-g & 0 & 0 \\[10pt]
0 & 1 & \dfrac{C_{z_\rho}}{h_0}/a \\[10pt]
0 & 1 & 0 \\[10pt]
0 & b\,\dfrac{c}{2U_0}(C_{m_{\dot\theta}} + C_{m_{\dot\alpha}}) & b\,\dfrac{c}{2U_0}\,C_{m_{\dot\alpha}}\dfrac{C_{z_\rho}}{h_0}/a \\[10pt]
U_0 & 0 & 0
\end{bmatrix} \tag{2-3}
$$

36

with

$$a = \frac{mU_0}{qS} \text{ , and } \quad b = \frac{qSc}{I_y} \quad .$$

The matrices of the elastic motion are defined

$$\underline{A}_j = \begin{bmatrix} 0 & 1 \\ -\omega_j^2 & -2d_j\omega_j \end{bmatrix} \quad j = 3,4,5,6 \quad (2-4)$$

and the $\underline{0}$ signify matrices all of whose values are zero.

Continuing, we define the control sensitivity matrix $\underline{B}$ as

$$\underline{B}' = [0 \quad C_{z_\delta}/a \quad 0 \quad b(C_{m_\delta} + \frac{c}{2U_0} C_{m_{\dot{\alpha}}} C_{z_\delta}/a) \quad 0 \quad 0$$

$$G_3/M_3 \quad 0 \quad G_4/M_4 \quad 0 \quad G_5/M_5 \quad 0 \quad G_6/M_6] \quad . \quad (2-5)$$

It is easily seen that Equations (1-17), (1-20), (1-21), (1-22), and (1-23) can be combined in the matrix form

$$\underline{\dot{x}}(t) = \underline{A}\underline{x}(t) + \underline{B}\delta(t) \quad . \quad (2-6)$$

A schematic representation of the system is shown in Figure 5.
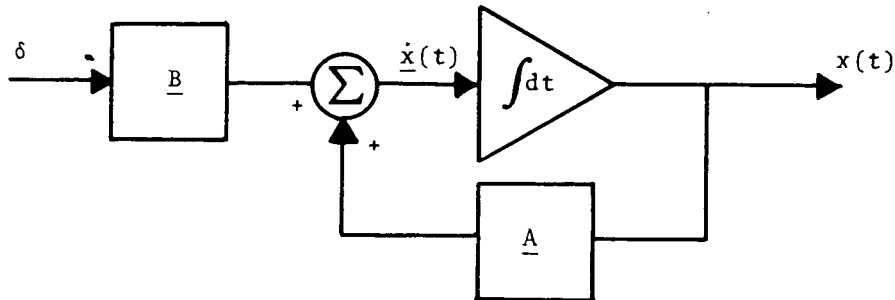

Figure 5: Block Diagram of System of Equation (2-6).

The cost functional can similarly be put into matrix notation involving the integral of a quadratic form. Let us construct the 13 x 13 matrix $\underline{L}$ as follows:

$$L_{3,3} = c_R M_2$$

$$L_{5,5} = c_R M_1 \qquad\qquad (2\text{-}7)$$

$$L_{2j,2j} = c_F M_j \omega_j^4 \qquad j = 3,4,5,6$$

and all other components of L are zero. We define the 12 x 1 matrix $\underline{N}$ as

$$\underline{N}' = \begin{bmatrix} 0 & 0 & 0 & 0 & 0 & -c_F \omega_3^2 G_3 & 0 & -c_F \omega_4^2 G_4 \end{bmatrix}$$

$$\begin{bmatrix} 0 & -c_F \omega_4^2 G_5 & 0 & -c_F \omega_4^2 G_6 & 0 \end{bmatrix} \qquad\qquad (2\text{-}8)$$

Finally construct the 1 x 1 matrix $\underline{R}$

$$\underline{R} = \sum_{n=3}^{6} \frac{G_n^2}{M_n} \quad . \qquad\qquad (2\text{-}9)$$

With the matrices $\underline{L}$, $\underline{N}$, and $\underline{R}$ defined as above, the cost functional given in Equation (1-41) becomes

$$J = \int_0^T \begin{bmatrix} \underline{x}' & \delta \end{bmatrix} \begin{bmatrix} \underline{L} & \underline{N} \\ \underline{N}' & \underline{R} \end{bmatrix} \begin{bmatrix} \underline{x} \\ \delta \end{bmatrix} dt \qquad\qquad (2\text{-}10)$$

and the control problem can be fully stated as follows: minimize J subject to Eq. (2-6).

38

A solution for the problem exists provided that the matrix $\underline{L}$ is non-negative definite, $\underline{R}$ is positive definite, and $\underline{L} - \underline{N}\underline{R}^{-1}\underline{N}'$ is non-negative definite. Equations (2-7), (2-8), and (2-9) substantiate that these conditions are met. The minimizing control $\delta^*(t)$ is given in the form of a feedback control law.

$$\delta^*(t) = -\underline{R}^{-1}(\underline{N}' + \underline{B}'\underline{K}(t))\underline{x}(t) \tag{2-11}$$

where $\underline{K}(t)$ satisfies the matrix Riccati equation

$$\dot{\underline{K}}(t) = -\underline{K}(t)\underline{A} - \underline{A}'\underline{K}(t) + (\underline{K}(t)\underline{B} + \underline{N})\underline{R}^{-1}(\underline{N}' + \underline{B}'\underline{K}(t)) - \underline{L};$$

$$\underline{K}(T) = 0 . \tag{2-12}$$

Furthermore, the minimum cost is given by

$$\underline{x}'(0)\underline{K}(0)\underline{x}(0) . \tag{2-13}$$

The reader is directed to Appendix D for the derivation of the optimal control.

A few words on the meaning of the control law are in order. The control law, Equation (2-11) is independent of initial values of the state. Hence δ^* is the minimum cost control for arbitrary initial conditions on $\underline{x}(t)$ which have been for this reason left unspecified in Eq. (2-6). As T, representing the time of cruise is large compared to response times of the system, the effect of the control is obviously to drive the state towards zero. With δ^* specified by Eq. (2-11), we can substitute into Eq. (2-6) to achieve the minimum cost trajectory

$$\dot{\underline{x}}^*(t) = (\underline{A} - \underline{B}\underline{R}^{-1}(\underline{N}' + \underline{B}'\underline{K}(t))\underline{x}^*(t) . \tag{2-14}$$

Note that the control δ* is memoryless, hence at any time t in the interval from 0 to T, we can consider the problem as minimizing the cost from t to T with initial state x(t).

So far the equations of motion for the airplane have neglected the input disturbances, random wind gusts. Let us now consider this effect and rewrite Eq. (2-6) as follows:

$$\dot{\underline{x}}(t) = \underline{A}\underline{x}(t) + \underline{B}\delta(t) + \underline{D}g(t) \tag{2-15}$$

where g(t) serves to model the random wind gusts, and $\underline{D}$ is the influence matrix for these gusts. The wind disturbances g(t) are clearly independent of the state, $\underline{x}(t)$, and the control δ(t). Furthermore, we may assume that the correlation times of g(t) are short compared with characteristic times of the system. This last assumption implies that knowledge of the gust history up to any time t, does not allow for effective prediction of future gust inputs far enough in advance to influence the control policy.

In terms of the stochastic differential equation of state Eq. (2-15), it is no longer valid to minimize the deterministic cost J. Rather, the control objective must now be to minimize the average or expected value of the cost

$$\tilde{J} = E \left\{ \int_0^T [\underline{x}' \quad \delta] \begin{bmatrix} \underline{L} & \underline{N} \\ \underline{N}' & \underline{R} \end{bmatrix} \begin{bmatrix} \underline{x} \\ \delta \end{bmatrix} dt \right\}. \tag{2-16}$$

An important result of stochastic control theory states that if the input disturbances are white noise, as assumed above, then the control to minimize J, given by Eq. (2-11) is identical to the minimizing control for $\tilde{J}$ subject to the stochastic system of Eq. (2-15)

The reader is directed to Reference 4, Chapter 14 for a more complete development.

The system, Equation (2-6) or (2-15), is time-invariant as the matrices A, B, and D, are constant, (the disturbance process, g(t) is assumed stationary) and all time varying signals will become very nearly ergodic shortly after the initial time. As the length of cruise, T, is extremely large compared to characteristic response times for the airplane, we would expect little change in either the total cost or the minimum cost trajectory for an increase in T. As T grows larger, the feedback gain matrix $\underline{K}(t)$ tends to a constant. The minimizing control is still given by Equation (2-11), but the matrix $\underline{K}$ is now given by the algebraic equation

$$-\underline{K}\underline{A} - \underline{A}'\underline{K} + (\underline{K}\underline{B} + \underline{N})\underline{R}^{-1}(\underline{N}' + \underline{B}'\underline{K}) - \underline{L} = \underline{0}. \tag{2-17}$$

Sufficient conditions for a well posed solution, i.e. a positive definite solution to the algebraic equation (2-17) and a finite minimum cost, include that the system
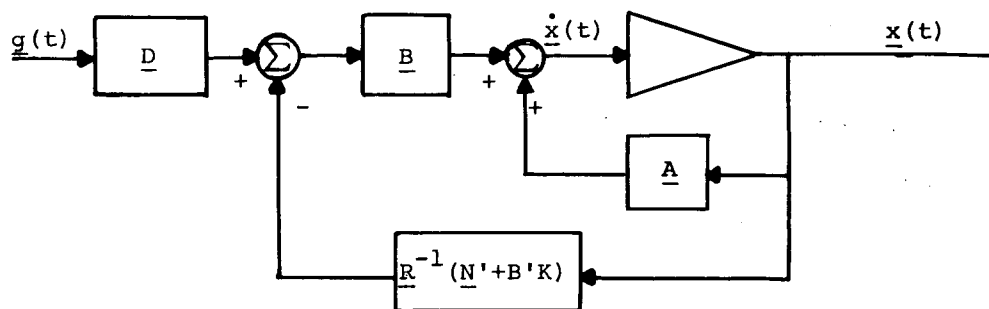

Figure 6. Block Diagram of System of Equation (2-15) with Closed Loop Minimum Cost Control

$$\dot{\underline{x}} = \underline{A}\underline{x} + \underline{B}u \; ; \; y = \underline{C}\underline{x} \qquad\qquad (2-18)$$

where $\underline{C}$ is the square root matrix of $\underline{L}$, i.e.

$$L = \underline{C}\underline{C}' \qquad\qquad (2-19)$$

(the existence of $\underline{C}$ is guaranteed for $\underline{L}$ symmetric and non-negative definite) be completely controllable and completely observable. The uncontrolled system need not be stable, yet the feedback controlled trajectory will be asymptotically stable. The SST model satisfies these conditions. The reader is directed to Reference 3 for further details.

B. Computer Implementation

The use of computers was restricted to two distinct areas for this study, data processing and simulation. The minimum cost control, Equation (2-11), was calculated by digital computer for different flight configurations. These results were then incorporated into an analog computer simulation where the effectiveness of the control could be observed.

The main thrust of the digital computer solution of the control problem lies in the solution of the time-invariant algebraic Riccati equation (2-17). The standard method is a backwards in time integration of the differential equation (2-12) until a steady state is achieved. For this analysis, a different solution technique was used based upon an algebraic algorithm developed by Potter. [Ref. 8]. The method devised by Potter involves calculating the eigenvalues and eigenvectors of the matrix $\underline{V}$,

42

$$\underline{V} = \begin{bmatrix} (\underline{A} - \underline{BR}^{-1}\underline{N}' & \underline{L} - \underline{NR}^{-1}\underline{N}' \\ \\ \\ \underline{BR}^{-1}\underline{B}' & -(\underline{A} - \underline{BR}^{-1}\underline{N}' \end{bmatrix} . \qquad (2\text{-}20)$$

The solution of Equation (2-17), which may be easily rewritten as

$$\underline{0} = -\underline{K}(\underline{A} - \underline{BR}^{-1}\underline{N}') - (\underline{A} - \underline{BR}^{-1}\underline{N}')'\underline{K} + \underline{KBR}^{-1}\underline{B}'\underline{K} - (\underline{L} - \underline{NR}^{-1}\underline{N}')$$

$$(2\text{-}21)$$

can be formulated in terms of the eigenvectors of $\underline{V}$. Furthermore, the eigenvalues of $\underline{V}$ can be shown to be the eigenvalues of the matrix $\underline{A} - \underline{BR}^{-1}(\underline{N}' + \underline{B}'\underline{K})$ i.e., the poles of the minimum cost closed loop system, Equation (2-14). These assertions are proved in Appendix E.

Potter's method, being an algebraic rather than an iterative scheme, has several advantages over the integration methods. The user need not be bothered choosing an integration step time, which may be crucial for the convergence of the solution. Also, the method is less sensitive to initial errors which tend to propagate in an iterative scheme. However a problem common to all digital calculations, limited precision, can have a devastating effect on the solution accuracy, and care must be taken to minimize the range of magnitudes of the input quantities through appropriate scaling.

Other subprograms necessary for the digital calculations included MAIN, an input-output routine to set up the matrices in the Riccati equation, and then calculate the feedback control gains; POTTER, which solves the Riccati equation; an eigenvalue-eigenvector routine called ALLMAT (authored by J. Rinzel and R. Funderlic of Union Carbide

Corp; Oak Ridge, Tenn.); and a matrix inversion subprogram TDINVR.

The analog simulation used the results of the digital calculations to examine the behavior of the controlled and uncontrolled systems. Due to the limited range of the analog computer, a number of extremely small parameters were set to zero. This, however, represented little loss of generality as the deleted quantities were orders of magnitude smaller than accompanying signals, and their removal ameliorated the problem of signals being swamped by noise. In addition to monitoring the effects of the control, the analog computer was a useful tool in assuring that the data inputs for the model were representative of predicted SST performance criteria.

CHAPTER 3

Application to the Model and Results

In this chapter the theories explained in the previous chapters
will be applied to an idealized model of the B-2707 prototype. The
first segment will deal with the physical aspects of the test airplane.
Results of the digital computations and analog simulation will be pre-
sented in later sections. Remarks are included in the final section.

A. Application to the Model

A.1. Generation of the Test Model

In preparing the analysis for computer implementation, it became
necessary to create an idealized version (Fig. 1) of the B-2707 pro-
totype aircraft. This model differs very slightly from the actual aircraft
in overall size, but as data on the mass distribution of the B-2707
was not available, it was necessary to postulate a distribution func-
tion for the model. (It should be clear that the problem formulation
is not dependent upon the specific mass distribution of the aircraft;
the latter enters solely as a data input and even then, smoothed
via integration.) A two phase mass distribution was chosen (constant
over the fuselage surface and constant over the lifting surfaces) as
the simplest form which would allow specification of two critical
parameters, the aircraft mass and center of gravity. These were chosen
to coincide with appropriate values for the actual B-2707, 11,700 slugs
and body station (B.S.) 2400 inches respectively.

To facilitate calculation of aircraft properties, the model was
partitioned by the superposition of a rectilinear grid into approximately
seventy-five segments. The extreme forward and aft fuselage sections,

comprising the first five hundred (500) inches and last two hundred
(200) inches of the body were excluded from further consideration.
These fuselage extensions are uninhabited (the crew compartment begins
at B.S. 560) and vibration mode data was unavailable for them. Modal
deflection was determined by averaging the deflection at the four lattice
points of each segment, and was assumed constant over the segment.

The generalized masses M_n and generalized force coefficients,
G_n (generalized force per unit elevator deflection) were calculated for
the flexure modes by integrating over the grid of the aircraft model.
The manufacturer's mode shapes shown in Figure 2 were used as the
normalized deflection modes for these integrations. The two sets of
parameters, M_n and G_n, together with the modal frequencies were pre-
calculated and fed into the digital programs as input. In addition,
to compensate for the structural damping present in the flexure dynamics,
but ignored in the derivation of Equation (1-17), a term corresponding
to a damping ratio of 0.03 was included in each of the equations of
flexure motion.

A.2 Flight Environment and Parameters

For the purposes of this investigation, the aircraft was assumed
to be in steady state cruise. The altitude and mach number of cruise
were chosen to be representative of proposed SST operating conditions,
65,000 feet, and Mach 2.7 respectively. As the speed of sound at this
altitude is 967 feet per second, the aircraft velocity is 2600 feet
per second. The mean air density at 65kft is 1.78×10^{-4} slugs per
cubic foot yielding a dynamic pressure of 602 slugs per foot-second
squared (lbs/ft^2). The reader desiring the calculations of these and
further quantities is directed to Appendix B.

The mass distributions over the wings and fuselage were calculated
to be 0.0042 and 0.0163 slugs/sq. in. respectively, and the lifting

surface of the model is computed to be 6680 square feet. The reference
wing chord was chosen to be 50 feet yielding a pitching moment of
inertia of 1.875×10^7 slug-ft^2. With these aircraft parameters at
hand, the lift and drag coefficients are readily calculated as 0.093
and 0.541×10^{-2}. From these values, the equilibrium angle of attack
becomes 0.058 radians, or approximately 3.3 degrees.

The stability derivatives appearing as coefficients in Equations
(1-20) thru (1-23) and examined in Appendix B can be calculated (or
in some cases approximated) from the parameters determining the flight
environment above. For the idealized B-2707 model, these coefficients
have the values (from the defining equations of Appendix B):

$$
\begin{array}{llll}
C_{x_u} & = & -0.0108 & \qquad C_{m_{\dot{\alpha}}} & = & \text{negligible} \\[2ex]
C_{z_u} & = & -0.186 & \qquad C_{m_{\dot{\theta}}} & = & -3. \\[2ex]
C_{m_u} & = & \text{negligible} & \qquad C_{z_\rho} & = & -0.093 \\[2ex]
C_{z_\alpha} & = & -1.6 & \qquad C_{z_\delta} & = & -0.144 \\[2ex]
C_{x_\alpha} & = & -0.093 & \qquad C_{m_\delta} & = & -0.192 \\[2ex]
C_{m_\alpha} & = & -0.2 &
\end{array}
\tag{3-1}
$$

Moving for a moment to the flexure motion, the generalized
masses, Equation (1-18), were computed via integration over the par-
titioned model. As by convention, we have designated the aircraft
mass and pitching moment of inertia as M_1 and M_2 respectively. The

remaining generalized masses associated with the flexure modes (measured in slugs) are

$$[M_3, M_4, M_5, M_6] = [1300, 63.9, 411, 726] .$$ (3-2)

Similarly, the generalized force coefficients, Equation (1-33), are computed via integration over the elevators of the partitioned model (See Figure 1), and for this flight condition take on the values. (measured in lbs/deg elevator deflection)

$$[G_3, G_4, G_5, G_6] = [5290, -1500, -2330, -616].$$ (3-3)

It should be noted that the Equations of rigid body dynamics (1-20) thru (1-23) and hence the matrix $\underline{A}_1$ defined by Equation (2-3), are based upon the angle perturbations being measured in radians. For computational reasons dealing with scaling, it is advantageous to measure angles in degrees. Therefore several entries in the $\underline{A}_1$ matrix need to be adjusted by the radian to degree scale factors, 57.296. Henceforth, we will use the units common to the computer implementation of the model; velocity is feet per second, angles of attack, pitch and elevator deflection are measured in degrees, altitude is in feet and flexure deformations are measured in feet, and flexure frequencies are radians per second. Designating insignificant or negligible terms by *, the matrix $\underline{A}_1$ becomes

$$\underline{A}_1 = \begin{bmatrix} -1.43\text{x}10^{-3} & -0.546 & -0.562 & 0 & 0 \\ * & -0.212 & 0 & 1 & * \\ 0 & 0 & 0 & 1 & 0 \\ * & -2.14 & 0 & -0.31 & * \\ 0 & -45.4 & 45.4 & 0 & 0 \end{bmatrix}$$ (3-4)

and the remaining non-zero blocks of the $\underline{A}$ matrix, the matrices of elastic motion are:

$$\underline{A}_3 = \begin{bmatrix} 0 & 1 \\ -85.2 & -0.554 \end{bmatrix} \quad \underline{A}_4 = \begin{bmatrix} 0 & 1 \\ -200. & -0.848 \end{bmatrix}$$

$$\underline{A}_5 = \begin{bmatrix} 0 & 1 \\ -259. & -0.965 \end{bmatrix} \quad \underline{A}_6 = \begin{bmatrix} 0 & 1 \\ -568. & -1.43 \end{bmatrix} . \tag{3-5}$$

The control sensitivity matrix B, defined by Equation (2-5) takes on the value

$$\underline{B}' = [0 \quad 0.0191 \quad 0 \quad -2.03 \quad 0 \quad 0 \quad 4.06 \quad 0$$

$$-23.5 \quad 0 \quad -5.66 \quad 0 \quad -0.848 \ ] . \tag{3-6}$$

The cost, defined in Equation (1-41) has a variable element, the ratio of C_R to C_F, which allows for a range of minimum cost controllers to be specified. For the digital computation of the feedback control gains, these two parameters were normalized so that C_F was identical to unity and the weighting coefficient for the costs attributable to rigid body motion, denoted as the cost ratio, was defined

$$CR = C_R/C_F. \tag{3-7}$$

In this completely equivalent formulation of the quadratic cost functional, the matrix $\underline{N}$, defined in Equation (2-8) becomes

$$\underline{N}' = [0 \quad 0 \quad 0 \quad 0 \quad 0 \quad -4.5 \times 10^5 \quad 0 \quad 3.0 \times 10^5$$

$$0 \quad 6.02 \times 10^5 \quad 0 \quad 3.50 \times 10^5 \quad 0]. \qquad (3\text{-}8)$$

The diagonal of the $\underline{L}$ matrix, Eq. (2-7), takes on the values

$$\underline{L} = [0 \quad 0 \quad 5.71 \times 10^3 \text{CR} \quad 0 \quad 1.17 \times 10^4 \text{CR} \quad 9.45 \times 10^6$$

$$0 \quad 2.55 \times 10^6 \quad 0 \quad 2.75 \times 10^6 \quad 0 \quad 2.34 \times 10^8$$

$$0 \;]. \qquad (3\text{-}9)$$

Finally, the $\underline{R}$ matrix, defined in Equation (2-10) becomes

$$\underline{R} = 7.05 \times 10^4. \qquad (3\text{-}10)$$

For reasons of computational accuracy, the elements of the $\underline{N}$, $\underline{L}$, and $\underline{R}$ matrices were further scaled down by a factor of 10^5 in the final digital programs.

B.   Results

B.1.   Digital Calculations

     Four different values of CR were used in the generation of digital solutions to the control problem in an attempt to view the effect of this parameter on the behavior of the closed loop feedback system. As CR varied from 0.05 to 100., with intermediate values of 1., and 10., the relative weightings assigned to rigid body and flexure perturbations varied by a factor of 2000. The particular values for CR were chosen

arbitrarily and in no way represent an exhaustive set or range of cost strategies. Furthermore, it should be clear that each value of CR leads to its own minimum cost solution. By varying CR we are not searching for an extremum again, but rather only viewing the consequences of a set of minimum cost trajectories.

The major computational effort of the digital program lies in the solution of the algebraic Riccati equation, Equation (2-17), which is used to generate the minimum cost feedback gains

$$\underline{fb} = -\underline{R}^{-1}(\underline{N}' + \underline{B}'\underline{K}) \qquad\qquad (3\text{-}11)$$

presented in Table 1. As CR increases, the rigid body influence on the control grows, as evidenced by the increases in fb_α, fb_θ, $fb_{\dot\theta}$, and fb_h. However, of the flexure motion, only the feedback gain for the first mode shows an appreciable decrease. The gains for the third and fourth modes instead increase with CR. This situation is counterintuitive at least, and helps to point out some of the subtleties encountered in generating minimum cost feedback controllers.

As stated in Chapter 2 and in Appendix D, the solution of the algebraic Riccati equation also yields the poles of the closed loop minimum cost trajectory. These pole locations have been plotted in Figure 7. The reader is cautioned that this diagram should not be interpreted as a root locus. The points plotted represent the poles of five distinct systems, not merely one system with a changing loop gain. Although only one parameter, CR, is varying in four of the systems, this parameter is involved in the closed loop system function in a far from trivial way. Secondly, and less profound, the reader should note the differences in scale between the Re(s) and Im(s) axes, chosen to help illustrate the pole locations.

$$
\begin{bmatrix}
fb_u \\
fb_\alpha \\
fb_\theta \\
fb_{\dot\theta} \\
fb_h \\
fb_{\xi_3} \\
fb_{\dot\xi_3} \\
fb_{\xi_4} \\
fb_{\dot\xi_4} \\
fb_{\xi_5} \\
fb_{\dot\xi_5} \\
fb_{\xi_6} \\
fb_{\dot\xi_6}
\end{bmatrix}
=
\overset{\underline{\text{CR}=0.05}}{
\begin{bmatrix}
6.13\times10^{-5} \\
-6.19 \\
6.89 \\
0.427 \\
0.091 \\
10.4 \\
-0.178 \\
-2.64 \\
0.301 \\
3.69 \\
0.780 \\
10.7 \\
0.845
\end{bmatrix}}
;\;
\overset{\underline{\text{CR}=1.0}}{
\begin{bmatrix}
1.15\times10^{-5} \\
-22.6 \\
25.0 \\
1.14 \\
0.407 \\
9.05 \\
-0.573 \\
-1.64 \\
0.334 \\
5.92 \\
0.723 \\
13.1 \\
0.781
\end{bmatrix}}
;\;
\overset{\underline{\text{CR}=10}}{
\begin{bmatrix}
1.25\times10^{-5} \\
-61.6 \\
67.9 \\
2.41 \\
1.28 \\
6.72 \\
-0.872 \\
-0.607 \\
0.350 \\
7.81 \\
0.664 \\
15.2 \\
0.708
\end{bmatrix}}
;\;
\overset{\underline{\text{CR}=100}}{
\begin{bmatrix}
8.43\times10^{-4} \\
-172. \\
188. \\
5.20 \\
4.12 \\
2.66 \\
-1.05 \\
0.724 \\
0.349 \\
9.93 \\
0.515 \\
17.5 \\
0.605
\end{bmatrix}}
$$

TABLE 1. Feedback Gains

As the uncontrolled system is block diagonalizable, [See Equation (2-2)] we can interpret the poles of this system in terms of its parallel subsystems. Referring to Figure 7, the four poles with imaginary points greater than 9 are precisely the frequencies of the four flexure modes. The remaining two uncontrolled pole pairs together with the real pole at -1.43×10^{-3} corresponding to u, the forward speed perturbation, represent the longitudinal group rigid body motion. The pole at the origin is but one of a pair related to the two states, θ and h, which are integrals of other states and devoid of feedback. The complex pole at (-.26, ±1.46) represents the short period mode, and as noted in Chapter 1 Section B, is the dominant second order system in angle of attack and pitch rate. [See Equations (1-24),(1-25)].

Im(s)

26

24

22

20

18

16

14

12

10

8

6

4

2

0

KEY

Uncontrolled system o

CR = 0.05 +

CR = 1.0 Δ

CR = 10. □

CR = 100. ×

NOTES

1. A cluster of symbols indicates that the true values lie too closely to-gether to be discerned at this scale, and should be taken coincidend at the center of the cluster.

2. All five systems exhibit a real pole at the point $(-1.43 \times 10^{-3}, 0)$, not shown on this graph.

x□
Δ+

x□
Δ+

x□
Δ+

o

o

o

o

o

×

□

Δ

+

×

□ □
×

Δ

+

□

Δ

+

o

-6   -5   -4   -3   -2   -1   0

-Re(s)
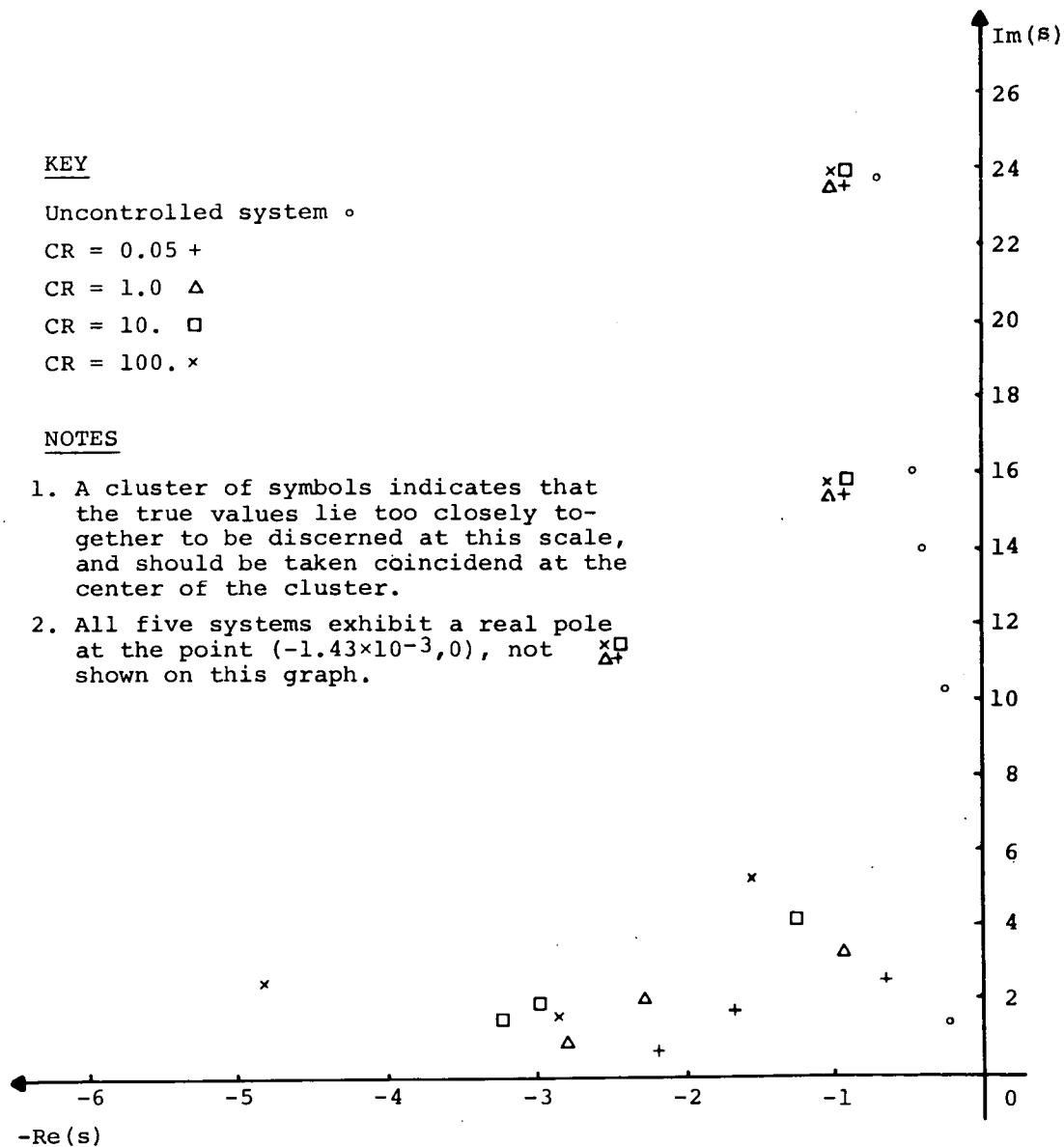
Figure 7. Poles of Uncontrolled and Minimum Cost Feedback Controlled Systems for Different Values of Cr. (Only Pole Location with Im(s)>0 Indicated for Complex Conjugate Pairs)

B.2 Analog Output

The open loop system model of Equation (2-6), was simulated on an analog computer. As the computer was of limited voltage range, considerable scaling was necessary before the simulation could be implemented. The negligible terms of the block system matrix $\underline{A}_1$, Equation (3-4), were set to zero as their slight magnitude precluded precise representation on the machine. The block diagram for the simulated system is shown in Figure 8. The feedback gains from the solution of the control problem were incorporated into the simulation for the CR = 1 and CR = 100 trials, yielding models of the minimum cost feedback controlled trajectory, Equation (2-14), for these cases.

Flight disturbances were simulated in a number of ways. First a standard elevator pulse of magnitude 5° for a duration of one second was used as a test input. This input is effective as a means of exciting both rigid and flexible body modes and demonstrates the ability of the autopilot to damp these modes. However, the elevator pulse is not representative of gust inputs and is not effective in demonstrating the trade-off of flexible body acceleration and rigid body displacement. Hence, responses were obtained for a standard set of initial conditions representing an initial nose up rotation of the aircraft by 5°. The resulting responses for CR = 1 and CR = 100 vividly demonstrate design trade-offs. Finally a vertical gust represented by the waveform 1-cos ωt was used to illustrate the design trade-off as it would apply to the gust input case.

We consider the elevator pulse input first. It is represented as

$$\delta_0(t) = 5(u_{-1}(t) - u_{-1}(t-1)) \tag{3-12}$$

where $u_{-1}(t-t_0)$ is the unit step at t_0. As the open loop system

54
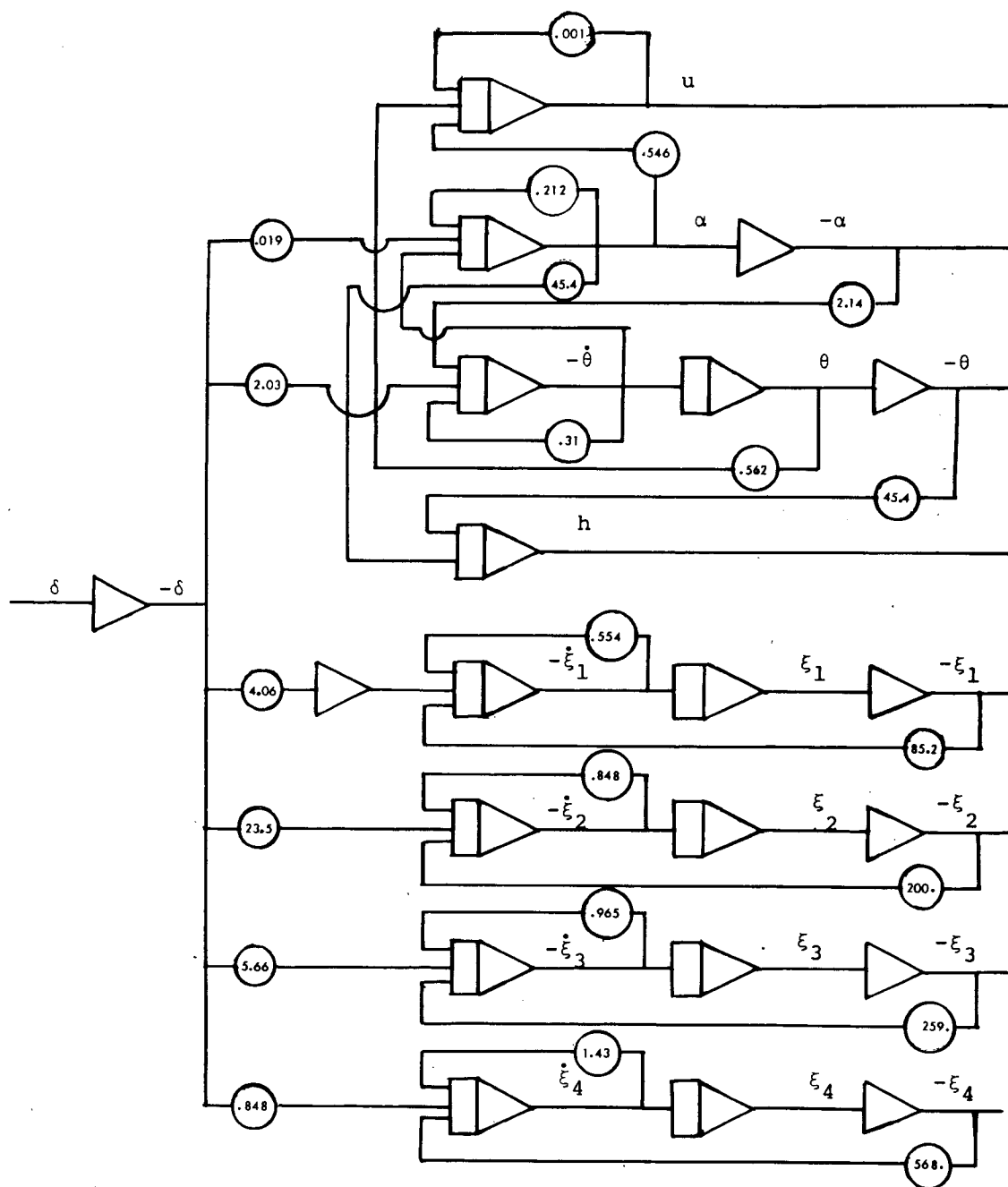
Figure 8. Block Diagram of Analog Simulation of Open Loop System

55

is composed of uncoupled subsystems, the responses to δ_0 completely illustrate the pole locations of Figure 7. The angle of attack perturbation represents the short period mode, a damped sinusoid of approximately 1.50 radians per second, decaying to zero, with a peak magnitude of five degrees. The pitch angle perturbation is similar in form and magnitude, but as the integral of the short period mode, it does not reach a final value of zero. Hence the net effect of the disturbance is to rotate the aircraft in space. As the glidepath angle $(\theta-\alpha)$ has a negative final value, the altitude decreases steadily. The θ and α time histories are shown in Figures 9 and 10. (For all analog computer output to follow the time scale will be one horizontal division per second; the vertical scale will be individually indicated. In all cases, the input disturbance to the system has been $\delta_0(t)$.)

The responses of the normal coordinates of the flexure motion (when the meaning is clear we will not make any distinction between the normal coordinates and the flexure motion they represent) are shown in Figures 11 thru 14. As the equation of motion of each flexure mode (Equation (1-17)) represents an uncoupled oscillator, the flexure responses are damped sinusoids corresponding to the uncontrolled system poles of Figure 7. The magnitude of each response is directly proportional to the corresponding control gain, G_n/M_n [See Equations (2-5) and (3-6)]. The large acceleration for the second mode is restricted to the extremes of the lifting surfaces [refer to Figure 2], and is due to the low generalized mass of this mode.

The pole locations of the minimum cost feedback controlled trajectories graphed in Figure 7 indicate roughly the system responses
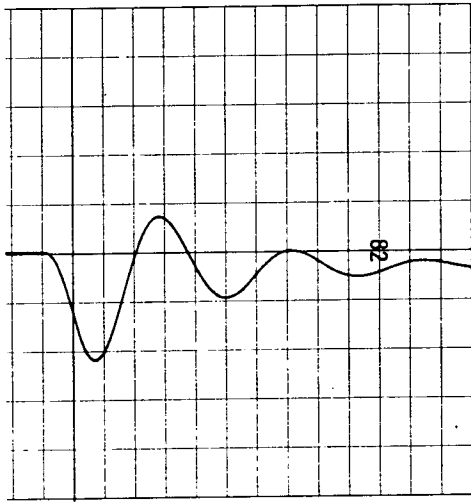
Figure 9. θ(t)-(uncontrolled)
Scale: 1/2 degree per line
Full scale: 12 1/2 degrees
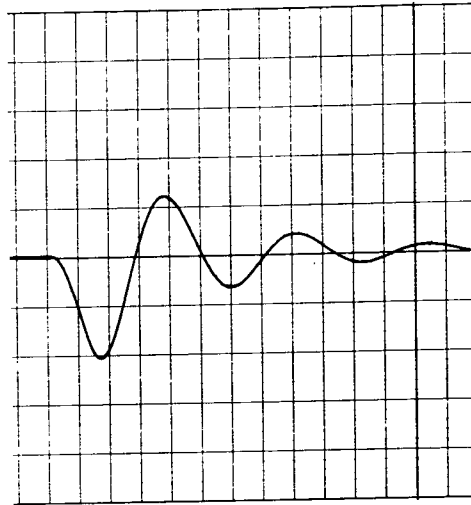
Figure 10. α(t) - (uncontrolled)
Scale: 1/2 degree per line.
Full scale: 12 1/2 degrees
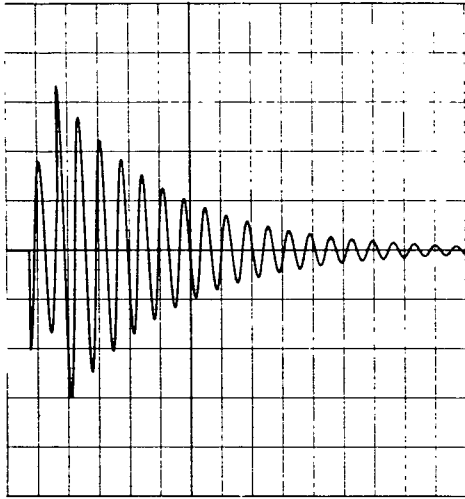
Figure 11. $-\ddot{\xi}_3(t)$ $_2$-(uncontrolled)
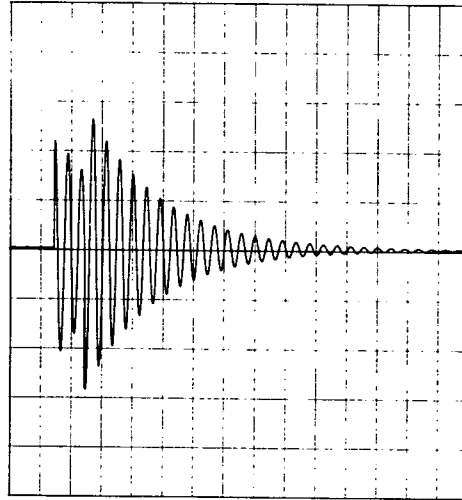Scale: 2 ft./sec^2 per line
Full scale: 50 ft./sec^2

Figure 12. $-\ddot{\xi}_4(t)$-(uncontrolled)
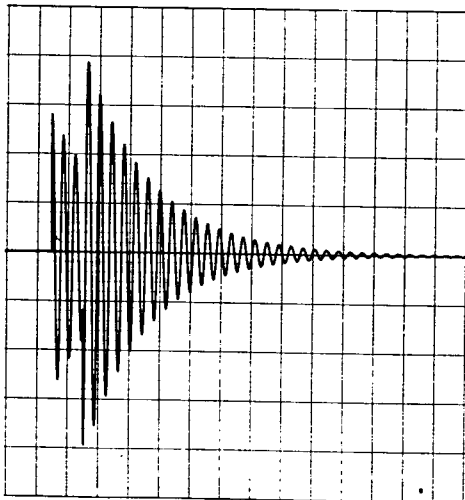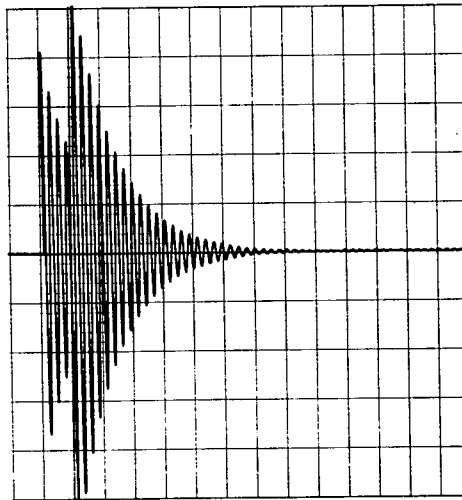Scale: 10 ft./sec^2 per line
Full scale: 250 ft./sec^2

Figure 13. $-\ddot{\xi}_5(t)$-(uncontrolled)
Scale: 2 ft./sec^2 per line.
Full scale: 50 ft./sec^2

Figure 14. $-\ddot{\xi}_6(t)$-(uncontrolled)
Scale: 0.2 ft./sec^2 per line.
Full scale: 5 ft./sec^2

to be expected from the analog simulations. In both the CR = 1 and

CR = 100 trials the poles corresponding to the three high frequency

flexing modes are coincident, hence we would expect the responses of

$\ddot{\xi}_4$, $\ddot{\xi}_5$, and $\ddot{\xi}_6$ to be nearly similar from one simulation to the next.

For the first mode however, the change in pole location with increasing

CR indicates that the fundamental frequency of this response will also

increase, with the damping ratio remaining approximately constant.

Similarly, the frequency content of the short period and altitude

responses increases with CR. As CR gets larger, from Table 1 we see

that the feedback gains grow, hence the total loop gain increases and

responses tend to be faster.

The pitch angle history, $\theta(t)$ is shown for the CR = 1 simulation

in Figure 15. The pitch angle motion frequency along with that of

the angle of attack, Figure 16, is approximately three radians per

second, and considerably speeded up from the open loop short period

mode. The responses for θ and α are nearly identical as h(t), pro-

portional to the integral of their difference, is being quadratically

penalized. The rotations reach a peak magnitude just under four

degrees while the altitude perturbation, Figure 17, remains less than

twelve feet at its greatest.

The control history is shown in Figure 18. (Actually - $\delta(t)$ is

presented in the figures; when $-\delta(t)$ is positive, the elevator deflec-

tion is upwards). The discontinuities of $\delta_0(t)$ are evident on the

control history graph as the spikes at the initial time and one second

thereafter. The control is primarily sinusoidal in shape with a

basic frequency of about three radians per second, in close accord

with the pitch and angle of attack motion. The range of elevator

deflection for this minimum cost trajectory is large, nearly twelve

degrees on either side of the equilibrium zero point. (The large,
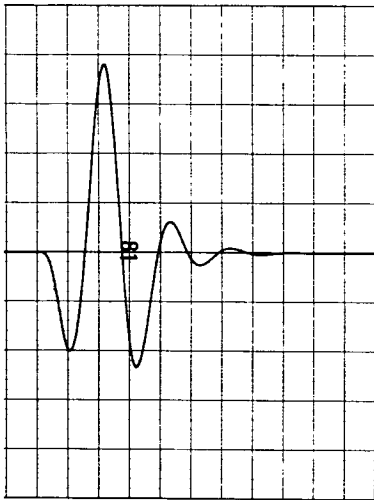
Figure 15. $\theta(t)$ (CR = 1)
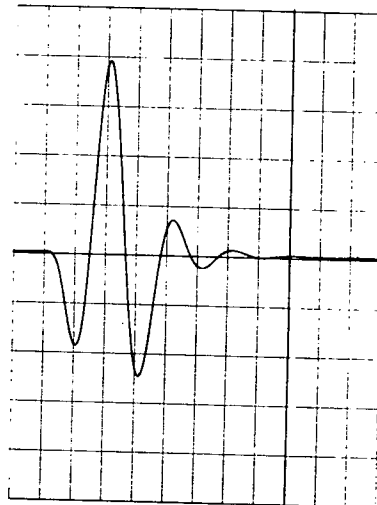Scale: 0.2 degree/line
Full scale: 5 degrees

Figure 16. $\alpha(t)$ (CR = 1)
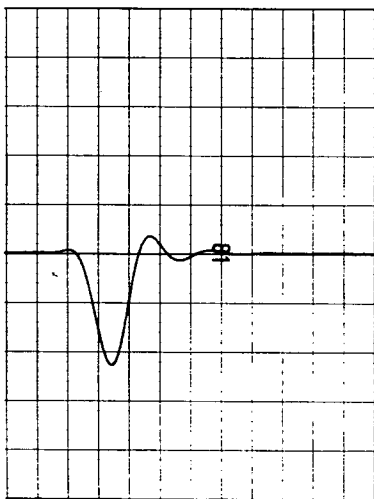Scale: 0.2 degree/line
Full scale: 5 degrees

Figure 17. h(t)(CR = 1)
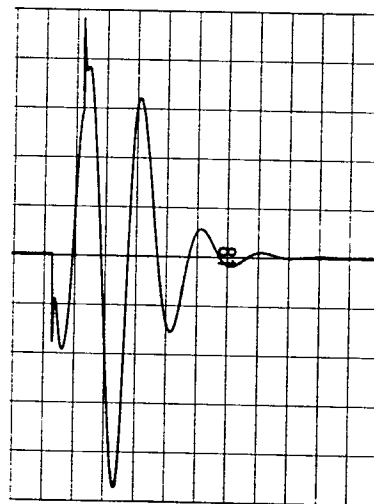Scale: 1 ft./line
Full scale: 25 ft.

Figure 18. $-\delta(t)$ (CR = 1)
Scale 0.5 degree/line
Full scale: 12 1/2 degrees

control effort is at least partly attributable to the specific form of the input.) In addition, a comparison of Figure 18 with Figures 15 and 16, show that after the external disturbance has been removed, the control δ follows the $\theta - \alpha$ motion, in that maxima of one align with maxima of the other. This behavior may be explained in terms of the feedback gains fb_θ and fb_α. From Table 1, regardless of CR, these gains are always in a ratio of approximately -1.1 to 1. Since the perturbation altitude rate is proportional to the flight path angle, or $\theta - \alpha$, the feedback to the controller from these two states can be interpreted as feedback of the flight path angle and additional feedback on the pitch. As $\theta - \alpha$ is very small, this feedback is roughly $0.1\ fb_\theta \theta$ and for the CR = 1 simulation, corresponds to $2.5\ \theta$.

The normal coordinates for the flexure accelerations, $\ddot{\xi}_3$ thru $\ddot{\xi}_6$, are presented in Figures 19 thru 22 respectively.* The CR = 1 controller significantly moves the pole corresponding to the first flexure mode, as shown in Figure 7 and documented in Figure 19. The peak acceleration for this mode has been reduced by about half, and the motion is quite irregular rather than sinusoidal.

As the second and third modes are quite close in frequency, it would be natural to expect that their responses in the closed loop system would be similar. This is the case, as evidenced by Figures 20 and 21. The magnitude of each mode has been reduced by about half over the open loop simulation and considerable damping has been added. Furthermore, each response has the appearance of the sum of two sinusoids, a fundamental of frequency about three radians per second and a higher frequency component, near fifteen radians per second. Finally, the acceleration of the fourth flexure mode indicates little effect

---

*(As in the case of the control history, $-\ddot{\xi}_n$ is actually graphed. These normal coordinates are abstract quantites and their sign depends solely on the orientation of the mode shapes from Figure 2.)
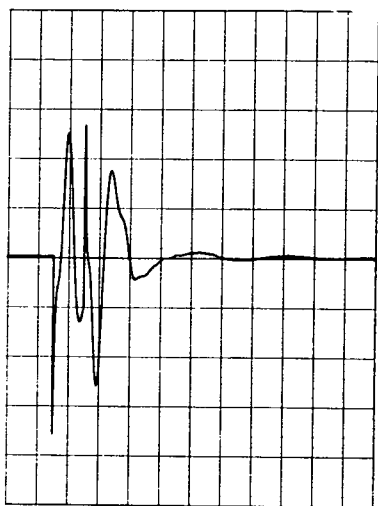
Figure 19. $-\ddot{\xi}_3(t)$ (CR = 1)
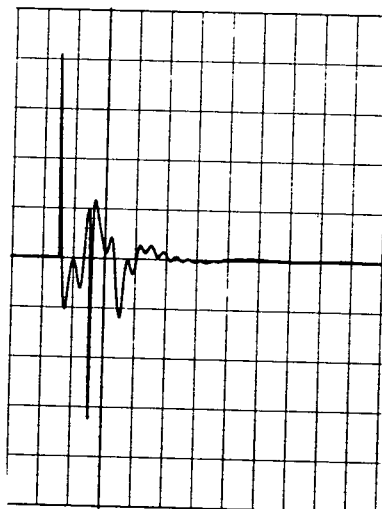Scale: 1 ft./sec.^{2} per line
Full scale: 25 ft./sec.^{2}

Figure 20. $-\ddot{\xi}_4(t)$ (CR = 1)
Scale: 5 ft./sec.^{2} per lines
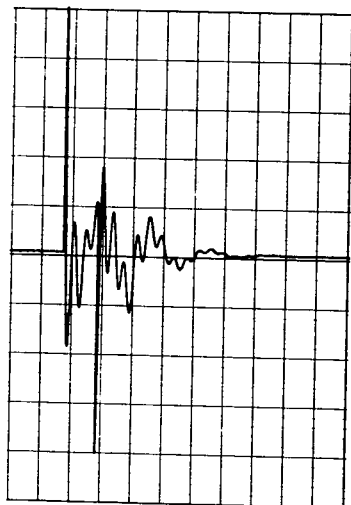Full scale: 125 ft./sec.^{2}

Figure 21. $-\ddot{\xi}_5(t)$ (CR = 1)
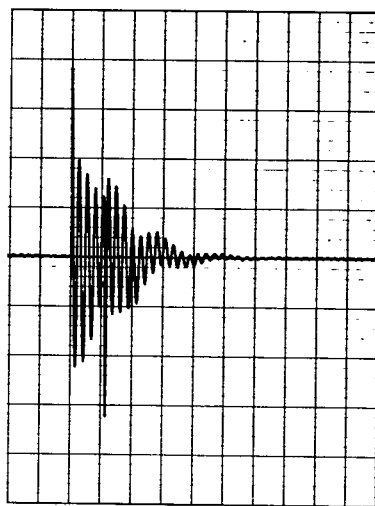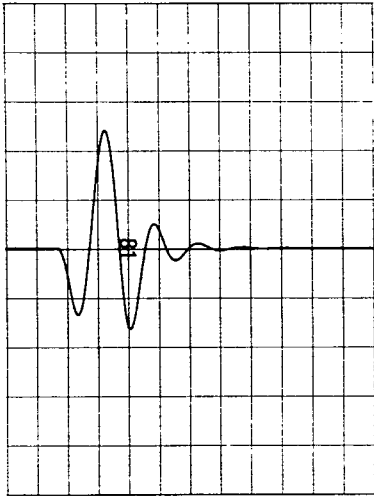Scale: 1 ft./sec.^{2} per line
Full scale: 25 ft./sec.^{2}

Figure 22. $-\ddot{\xi}_6(t)$ (CR = 1)
Scale: 0.2 ft./sec.^{2} per line
Full scale: 5 ft./sec.^{2}

62

Figure 23. θ(t) (CR = 100)
Scale: 0.05 degree/line
Full scale: 1.25 degrees
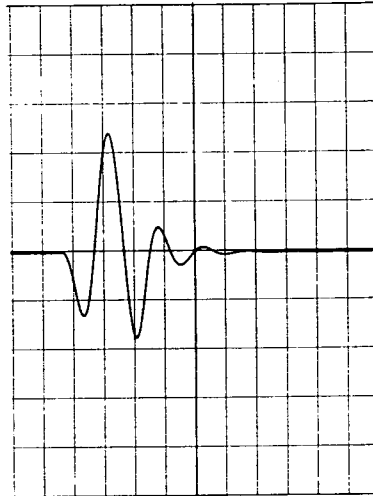

Figure 24. α(t) (CR = 100)
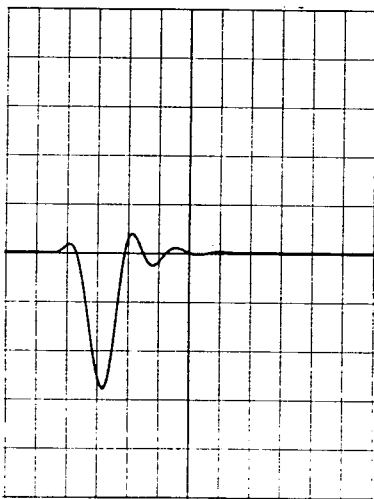Scale: 0.05 degree/line
Full scale: 1.25 degrees

Figure 25. h(t) (CR = 100)
Scale: 0.1 feet/line
Full scale: 2.5 feet
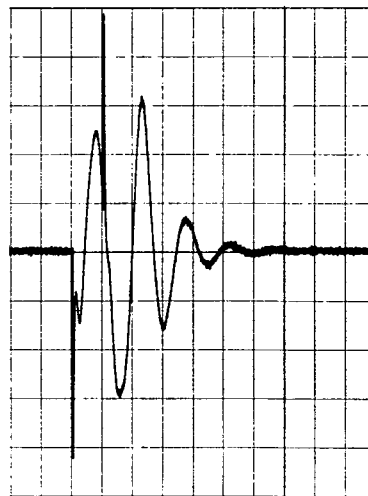

Figure 26. -δ(t) (CR = 100)
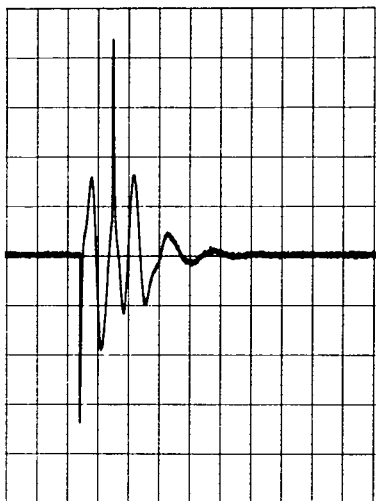Scale: 0.2 degree/line
Full scale: 5 degrees

Figure 27. $-\ddot{\xi}_3(t)$ (CR = 100)
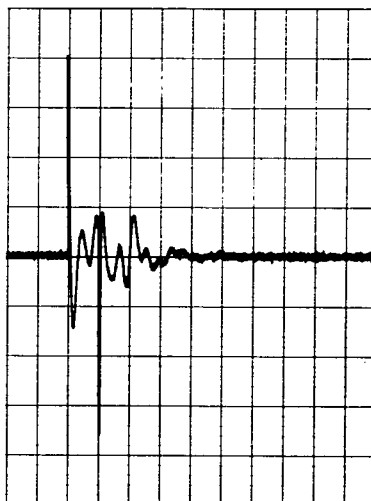Scale: 1 ft./sec.² per line
Full scale: 25 ft./sec.²

Figure 28. $-\ddot{\xi}_4(t)$ (CR = 100)
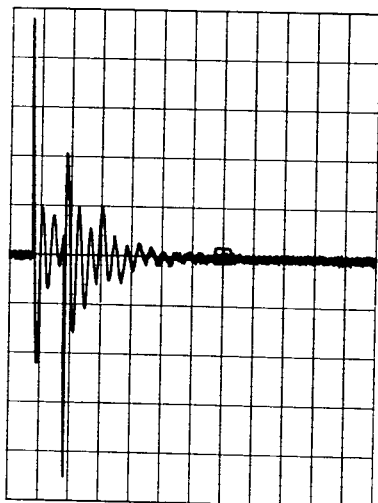Scale: 5 ft./sec.² per line
Full scale: 125 ft./sec.²

Figure 29. $-\ddot{\xi}_5(t)$ (CR = 100)
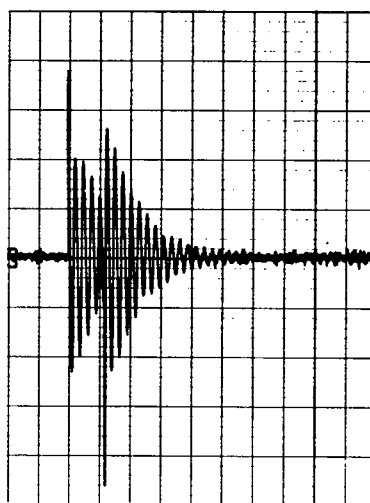Scale: 1 ft./sec.² per line
Full scale: 25 ft./sec.²

Figure 30. $-\ddot{\xi}_6(t)$ (CR = 100)
Scale: 0.2 ft./sec.² per line
Full scale: 5 ft./sec.²

64

of the control, except that the magnitude of the response has been diminished.

The system responses for the CR=100 trial agree with what was roughly intuited from the pole location map of Figure 7. The pitch and angle of attack motion, shown in Figures 23 and 24 is of similar form to that from the first simulation, although the fundamental frequency has increased to roughly four radians per second. More startling however, is the reduction in magnitude of the response, which is now under 0.6 degrees, nearly an 85% reduction over the CR = 1 simulation. Similarly the plunge motion, $h(t)$, shown in Figure 25 is dramatically reduced, in this case by an even larger margin. Here too, the basic frequency has been slightly increased. The control, $\delta(t)$, Figure 26, is still aligned with the $\theta - \alpha$ motion, and is of similar form to the control of the CR = 1 trial, Figure 18. However for CR = 100, the range of elevator deflection has been significantly diminished, and is now limited to five degrees.

From the plot of closed loop poles from Figure 7, we would not expect large changes in the responses of the higher frequency flexure modes as CR increases to 100. The graphs of $\ddot{\xi}_4$, $\ddot{\xi}_5$, and $\ddot{\xi}_6$, Figures 28, 29, and 30 show that this is indeed the case. The responses to the second and third modes are not quite as similar as in the CR = 1 trial. This is partially explained by the feedback gains fb_{ξ_4} and fb_{ξ_5}, which for CR = 100 do not act to cancel out the influence of these modes in the control. In each of these three responses, the magnitude is close to that for the CR = 1 simulation. The first flexure mode response, Figure 27, is likewise roughly the same magnitude as for the first trial. However, the CR = 100 response is seen to be more regular, and of a higher fundamental frequency. For a different input disturbance we might expect the first mode to exhibit a larger response for the

higher cost ratio trial.

Finally, the sum of the flexure accelerations and the resultant displacement of the pitch and plunge motions were examined for both simulations at three points along the fuselage, B.S. -800, B.S. -2000, and B.S. -3200, corresponding to the forward, middle, and rear of the passenger compartment. The acceleration component of the nth node at the point (x,y) is given by $\phi_n(x,y)\ \ddot{\xi}_n(t)$. From Figure 2, we can read off the appropriate value of the coefficient $\phi_n(x,y)$ and the sum over the modes to achieve the total flexure acceleration. The rigid body displacement is computed by adding to the altitude perturbation the pitch angle multiplied by the pitching moment arm, $(x_{c.g.}-x)$.

The flexure accelerations for the CR = 1 simulation are given in Figures 31, 32, and 33. From Figure 2, we would expect the acceleration at the forward and middle fuselage areas to be dominated by the first flexure mode. Comparison of Figures 31 and 32 with Figure 19 tends to bear this out. The flexure acceleration at the rear of the passenger compartment is heavily dependent upon the higher frequency modes. At all three points, the accelerations are reduced to about half those present in the uncontrolled system, shown in Figures 43, 44, and 45.

The CR = 100 simulation yielded similar results for the total flexure accelerations, shown in Figures 37, 38, and 39. The magnitudes of the responses were indeed close to those for the lower cost ratio trial. Figure 27 illustrates the heavy dependence of the forward and middle area acceleration histories on the first flexure mode.

The rigid body displacements for both trials, CR = 1, presented in Figures 34, 35, and 36, and CR = 100, Figures 40, 41 and 42, are exceedingly similar in form. The B.S. - 800 response indicates the
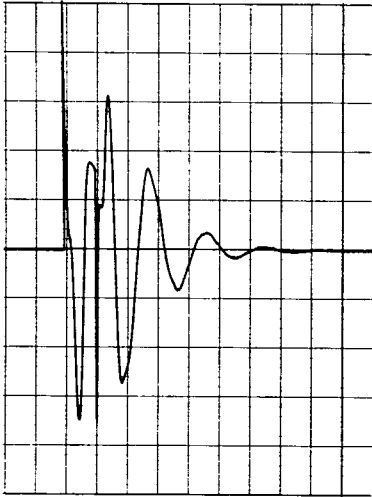
66

Figure 31. Flexure acc. at
         B.S. 800 (CR = 1)
Scale: 0.5 ft/sec.^{2} per line
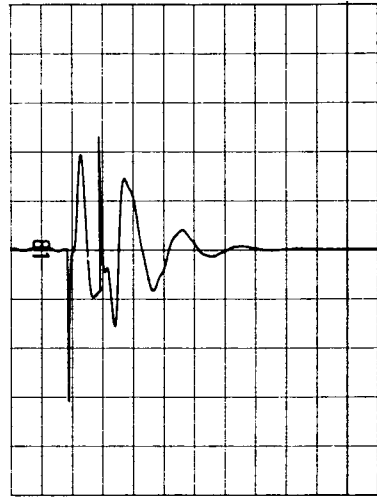Full scale: 12.5 ft./sec.^{2}

Figure 32. Flexure acc. at
         B.S. 2000 (CR = 1)
Scale: 0.5 ft./sec.^{2} per line
Full scale: 12.5 ft./sec.^{2}

Figure 33. Flexure acc. at
         B.S. 3200 (CR = 1)
Scale: 0.5 ft./sec.^{2} per line
Full scale: 12.5 ft./sec.^{2}

Figure 34. R.B. disp. at
         B.S. 800 (CR = 1)
Scale: 0.5 ft./line
Full scale: 12.5 ft.

Figure 35. R.B. disp. at
           B.S. 2000 (CR = 1)
Scale: 0.5 ft./line
Full scale: 12.5 ft.

Figure 36. R.B. disp. at
B.S. 3200 (CR = 1)
Scale: 0.5 ft./line
Full scale: 12.5 ft.
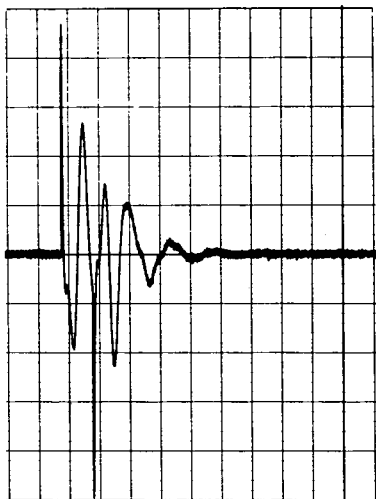
Figure 37. Flexure acc. at
           B.S. 800 (CR = 100)
Scale: 0.5 ft./sec.^{2} per line
Full scale: 12.5 ft./sec.^{2}

Figure 38. Flexure acc. at
           B.S. 2000 (CR = 100)
Scale: 0.5 ft./sec.^{2} per line
Full scale: 12.5 ft./sec.^{2}

68
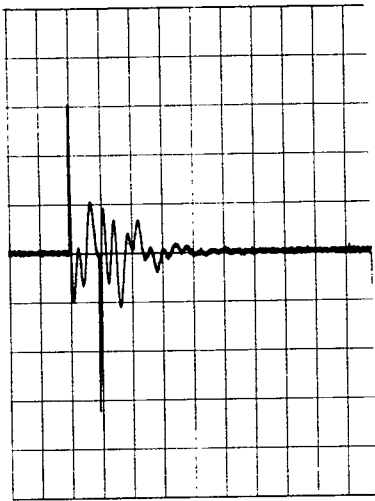
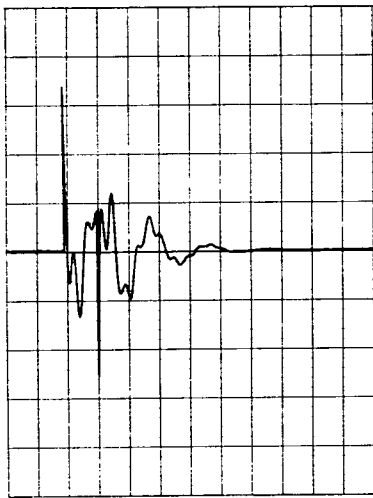Figure 39.   Flexure acc. at
                    B.S. 3200 (CR = 100)
Scale: 0.5 ft./sec.^{2} per line
Full scale: 12.5 ft./sec.^{2}
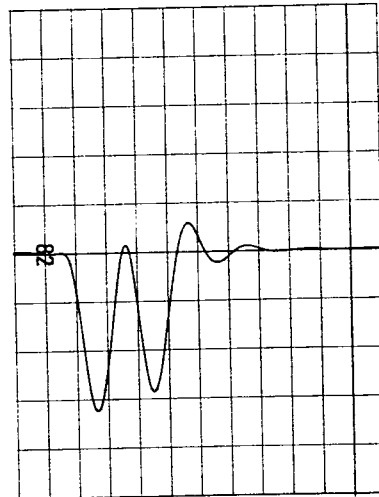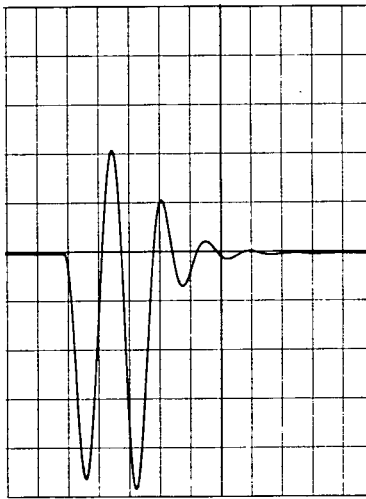
Figure 40. R.B. disp at
                    B.S. 800 (CR = 100)
Scale: 0.1 ft./line
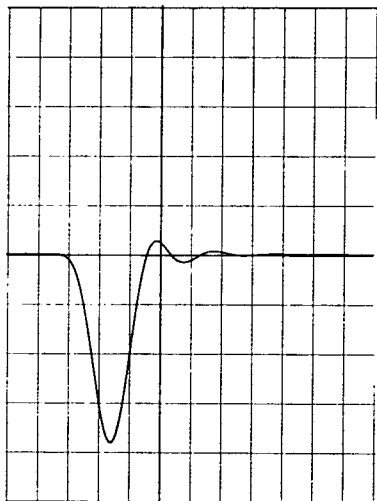Full scale: 2.5 ft.
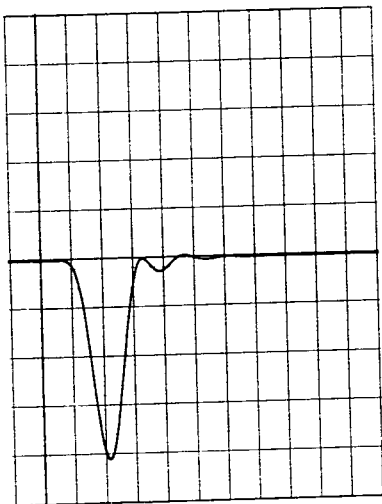
Figure 41.   R.B. disp. at
                    B.S. 2000 (CR = 100)
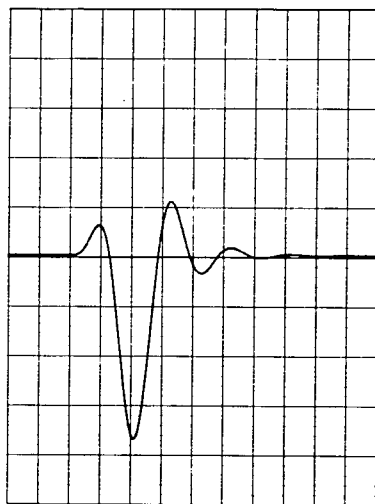Scale: 0.05 ft./line
Full scale: 1.25 ft.
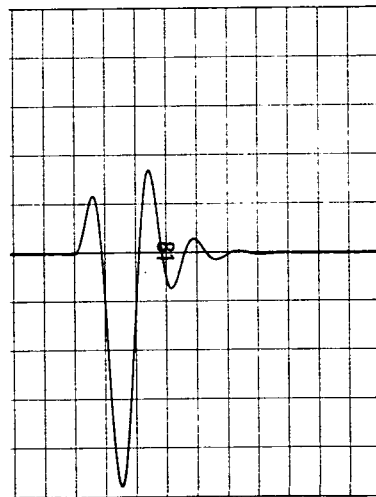
Figure 42. R.B. disp. at
                    B.S. 3200 (CR = 100)
Scale: 0.1 ft./line
Full scale: 2.5 ft.
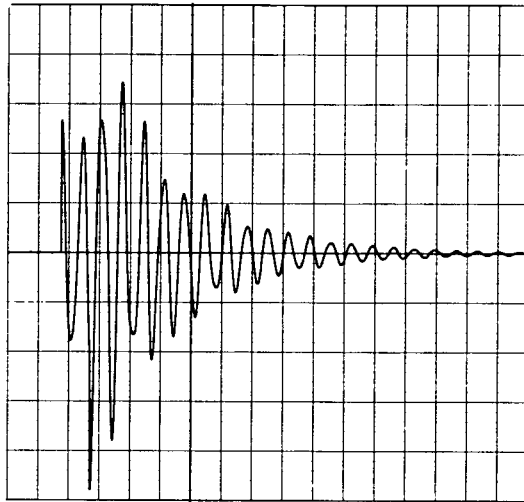
Figure 43. Flexure acc. at B.S. 800 (uncontrolled)
Scale: 1 ft./sec.^{2} per line
Full scale: 25 ft./sec^2
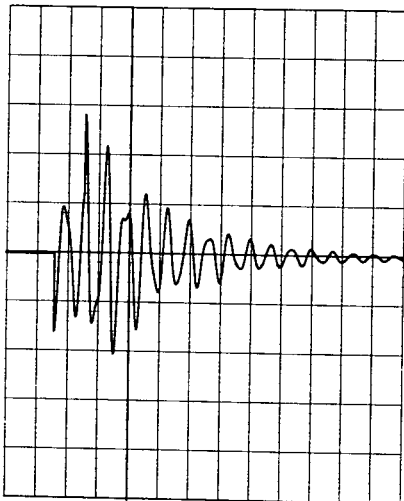
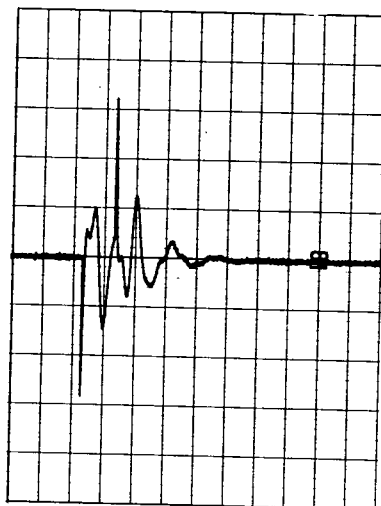Figure 44. Flexure acc. at
          B.S. 2000 (uncontrolled)
Scale: 1 ft./sec^2 per line
Full scale: 25 ft./sec^2
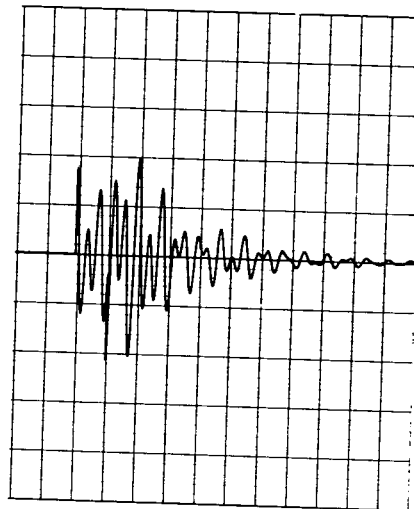
Figure 45. Flexure acc. at
          (B.S. 3200 (uncontrolled)
Scale: 1 ft./sec^2 per line
Full scale: 25 ft./sec^2

70

effect of the long moment arm (1600 inches) on this motion, while the middle fuselage response is almost entirely plunge motion. The B.S. -3200 response, with a moment arm of 800 inches is still basically the altitude perturbation. However the magnitudes of the response are decidedly different. At all three positions, the displacements for the CR = 1 simulation are at least three times as large as the corresponding displacement for the higher cost ratio trial.

As previously mentioned, the external input $\delta_0(t)$ is particularly successful in exciting the different modes of the aircraft, but less effective in contrasting the trade-offs in system performance for differing values of cost ratio. The results show a decided decrease in the rigid body perturbations for the CR = 100 trial; yet the flexure accelerations for the CR = 1 simulations are not appreciably smaller. The changes in response for changes in CR are more apparent when other means of simulating the input disturbance are used.

Figures 46 thru 49 illustrate the effect of non-zero initial conditions as input to the system. For these outputs, respresenting the rigid body displacements and flexure accelerations at the middle fuselage area (B.S. 2000), the initial angle of attack perturbation was set to five degrees. The initial pitch angle was adjusted to approximately 4.5 degrees so that the combined feedback from θ and α exactly cancelled out, preventing the immediate saturation of the analog computer. The non-zero initial displacement shown in Figures 46 and 48 is due to the effect of the positive pitch angle. Comparison of the results for the two cost ratios more readily indicates the trade-offs in system performance. The higher weighting on the rigid body excursions results in a reduction by over one half for this motion, [See Figures 46 and 48] but the price for this improved dynamics is an order of magnitude increase in flexure accelerations. [See Figures 47 and 49]
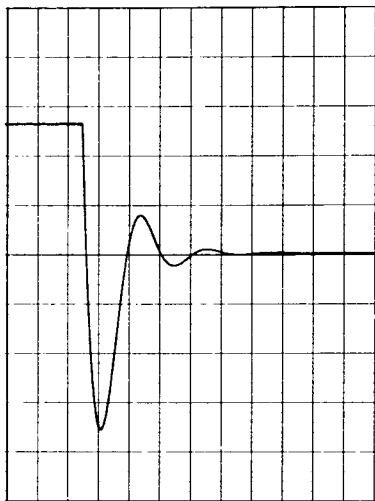
Figure 46.   R.B. disp. at
         B.S. 2000 (CR = 1)
      (from initial conditions)
Scale: 0.2 feet per line
Full scale: 5 feet
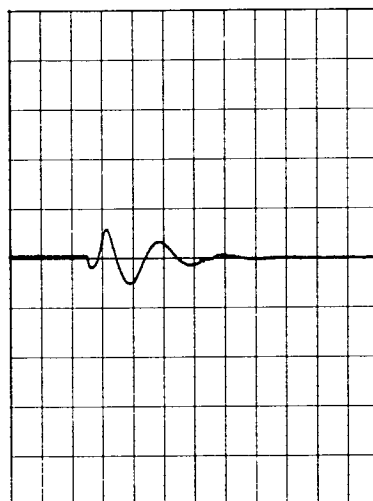
Figure 47. Flexure acc. at
         B.S. 2000 (CR = 1)
      (from initial conditions)
Scale: 0.2 ft./sec.^{2} per line
Full scale: 5 ft./sec.^{2}
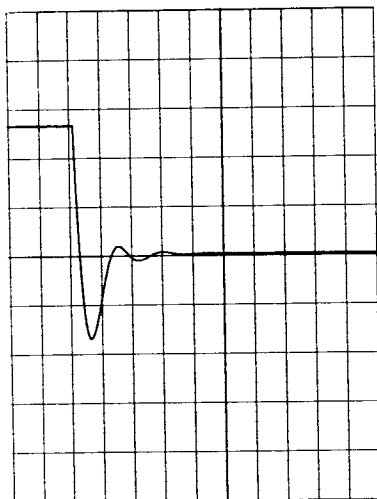
Figure 48.   R.B. disp. at
         B.S. 2000 (CR = 100)
   (from initial conditions)
Scale: 0.2 feet per line
Full scale: 5 feet
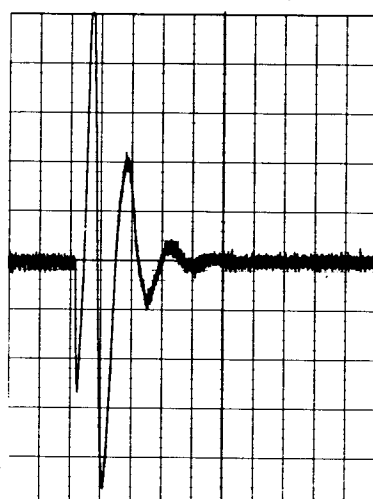
Figure 49. Flexure acc. at
         B.S. 2000 (CR = 100)
      (from initial conditions)
Scale: 0.2 ft./sec.^{2} per line
Full scale: 5 ft./sec.^{2}

72
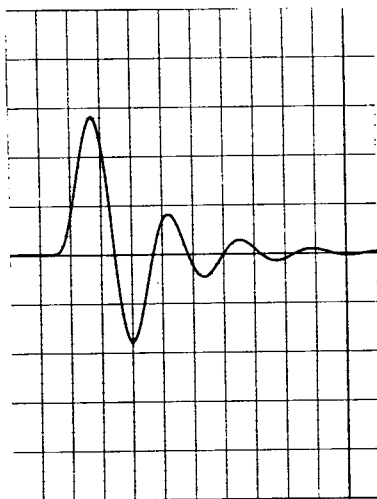
Figure 50. θ(t) (CR = 1)
Scale: 0.1 degree/line
Full scale: 2-1/2 degrees
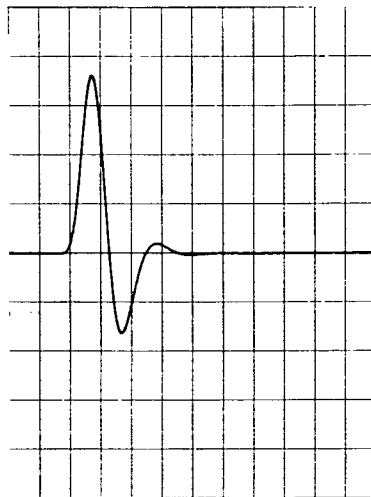
Figure 51. θ(t) (CR = 100)
Scale: 0.1 degree/line
Full scale: 2-1/2 degrees
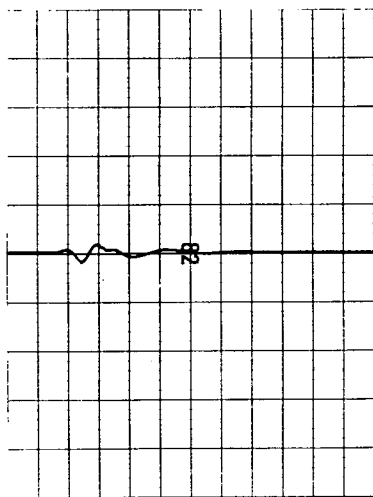
Figure 52. Flexure acc. at
B.S. 2000 (CR = 1)
Scale: 0.5 ft/sec.^{2} per line
Full scale: 12.5 ft./sec.^{2}
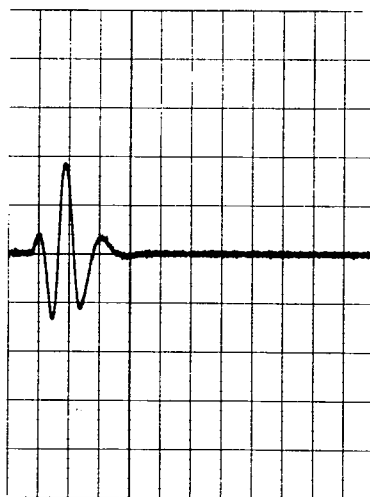
Figure 53. Flexure acc. at
B.S. 2000 (CR = 100)
Scale: 0.5 ft./sec.^{2} per line
Full scale: 12.5 ft./sec.^{2}

73
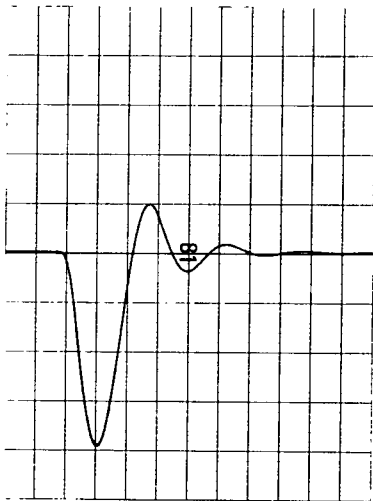
Figure 54.   R.B. disp. at
            B.S. 2000 (CR = 1)
Scale: 0.2 ft./line
Full scale: 5 ft.
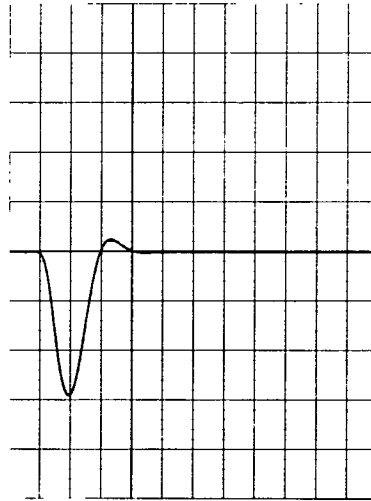
Figure 55. R.B. disp. at
            B.S. 2000 (CR = 100)
Scale: 0.2 ft./line
Full scale: 5 ft.

The characteristics of the specific responses are again at least partly attributable to the type of input disturbance employed. The initial conditions used were not effective in exciting the elastic motion of the airframe, and for the CR = 1 trial did not cause large control action. For the CR = 100 simulation, however, the higher body feedback gains resulted in a larger control effort which in turn excited the flexure modes.

Finally, a set of runs was made to simulate gust inputs. One cycle of the function 1 - cos ωt was used to represent a downward gust. The frequency utilized was 1 cycle per second placing the input near resonance of the controlled short period mode. Maximum gust velocity was 40 ft./sec. Figures 50 and 51 illustrate the pitch responses for the two cases CR = 1 and CR = 100. We note that as for the other input cases, the CR = 100 autopilot damps the pitch motion appreciably better than the CR = 1 autopilot. The initial positive pitch in both cases is the result of the aircraft weathercocking into the downward gust. Figures 52 through 55 show flexible body accelerations and rigid body displacements for the CR = 1 and CR = 100 cases at body station 2000. As expected, the rigid body motion is better controlled with CR = 100, however, the flexible body acceleration is larger by an order of magnitude than for CR = 1. Hence a relatively large penalty is paid, in terms of flexible body accelerations for better control of the rigid body displacements. Responses at other body stations were similar.

C. Remarks

The results of the previous section demonstrate the effect of the design parameter CR in the controlled system responses. The feedback control in both trials not only diminished the magnitude of the undesirable responses, but also lowered the basic frequency of the flexure

accelerations [compare Figures 30-33, 37-39, 43-45], which according to Figure 4 is a desirable end. If the cost ratio were increased further, we could expect better rigid body responses but a decrease in the ability to control the elastic deformations and to lower their frequency content. Diminishing CR would lead to the converse behavior. No particular value of CR is in an absolute sense best; but rather best according to the desires of the designer, who can use this parameter to influence the controller according to his own subjective preferences.

The particular entries of the cost for this investigation, flexure accelerations, and rigid body displacements, represent but one of many possible variations. There is no difficulty in including the displacements due to the elastic deformations of the structure, or the rigid body accelerations to the cost functional. Similarly there is no reason why one could not have additional cost ratio terms, representing preferential weightings on other responses.

Along another vein, the present model could be selectively simplified without significant degradation of the responses. The perturbation in forward speed, u, has been shown to contribute little to the model, in that it neither enters the cost nor the control to other but negligible degree. Hence Equation (1-20) could be omitted from the longitudinal group set and u dropped as a pertinent state variable. The fourth flexure mode seems little affected by the controller, and since it is of small magnitude, one interested in simplifying the model would delete the equations corresponding to this motion.

In solving the equations of elastic deformation, we made use of separability to derive equations for the mode shapes $\phi_n(x,y)$, and normal coordinates $\xi_n(t)$. The control problem then used these normal coordinates as state variables and developed a control as a linear combination of the normal coordinates and other states of the system.

76

If we wish to implement this controller, the rigid body perturbations are well understood and easily obtained for feedback purposes. The flight path angle, pitch angle, pitch rate, and altitude perturbation are available from onboard navigational aids, such as an inertial measurement unit. But how do we obtain the normal coordinates for feedback purposes?

A sketch of one method which could be implemented follows. Since the feedback controlled system, Equation (2-14) is linear, we can transform the system matrix $\underline{A} - \underline{BR}^{-1}(\underline{N}'+\underline{B}'\underline{K})$ into its Jordan canonical form. The resulting transformation will give us a new system

$$\dot{\tilde{\underline{x}}}(t) = \tilde{\underline{A}}\ \tilde{\underline{x}}(t) \tag{3-13}$$

where

$$\underline{A}-\underline{BR}^{-1}(\underline{N}'+\underline{B}'\underline{K}) = \underline{V}\tilde{\underline{A}}\underline{W} \tag{3-14}$$

and where $\underline{V}$ and $\underline{W}$ are orthonormal linear transformations involving the eigenvectors of $\underline{A} - \underline{BR}^{-1}(\underline{N}'+\underline{B}'\underline{K})$, and

$$\tilde{\underline{x}} = \underline{W}\underline{x}\ . \tag{3-15}$$

This new system of Equation (3-13) has the property that its state variables represent uncoupled subsystems corresponding to the eigenvalues of the system matrix $\underline{A} - \underline{BR}^{-1}(\underline{N}'+\underline{B}'\underline{K})$.

These eigenvalues are exactly those poles plotted in Figure 7. Since the elastic motion was assumed band limited, a finite number of accelerometers strategically placed along the aircraft would give us sufficient data to recover the normal coordinates. The output from the accelerometers could be filtered to isolate a frequency corresponding to one complex set of eigenvalues. The relation between $\tilde{\underline{x}}$ and $\underline{x}$ then tells us the amount of each state of $\underline{x}$ contained in a given

state of $\tilde{\underline{x}}$. Since we can measure the states of $\tilde{\underline{x}}$ (by integrating the filtered output from the accelerometers), we can thus obtain measurements for the states of $\underline{x}$, i.e. the normal coordinates.

APPENDIX A

Derivation of Equations of Flexure Dynamics

(The analyses of this section follow from Aeroelasticity, by
Bisplinghoff, Ashley, and Halfman.)

A.1. Differential Equations of Motion of a Slender Beam

The equations of motion for free (unforced) vibrations of a long
slender beam where rotary inertia effects and transverse shear defor-
mations have been neglected is

$$\frac{\partial^2}{\partial x^2}\left(EI\,\frac{\partial^2 w(x,t)}{\partial x^2}\right) + m(x)\,\frac{\partial^2 w(x,t)}{\partial t^2} = 0 \tag{A.1-1}$$

where $w(x,t)$ represents the displacement of the point x along the beam
at time t, EI is the bending stiffness, and $m(x)$ is the mass distribu-
tion along the beam. Equation (A.1-1) is easily derived from a consid-
eration of force and moment balance on an incremental element of the
beam.

Henceforth, we will dispense with this rather cumbersome notation
for derivatives and will adopt the following scheme:

$f'(\cdot)$ will signify $\frac{\partial}{\partial x}\,f(\cdot)$

$\dot{f}(\cdot)$ will signify $\frac{\partial}{\partial t}\,f(\cdot)$.

We note that Eq. (A.1-1) is separable, i.e. will admit solutions
of the form

$$w(x,t) = W(x)\,T(t). \tag{A.1-2}$$

Substitution of the above into Equation (A.1-1) yields

$$\frac{-\ddot{T}}{T} = \frac{(EI\cdot W'')''}{mW} \tag{A.1-3}$$

As x and t are independent variables, the quotients in Eq. (A.1-3) must also be independent of x and t. Equating these quotients to ω^2, the following ordinary differential equations are obtained:

$$\ddot{T} + \omega^2 T = 0 \qquad \text{(A.1-4)}$$

$$(EI \cdot W'')'' - m\omega^2 W = 0. \qquad \text{(A.1-5)}$$

Solutions to Eq. (A.1-5) are eigenfunctions and the values of ω are eigenvalues of the problem. These eigenfunctions are mutually orthogonal with respect to the mass distribution, $m(x)$, as shown below.

Assume W_m, W_n, ω_m, ω_n are two eigenfunctions and associated eigenvalues satisfying Eq. (A.1-5). Then

$$(EI \cdot W_m'')'' - m\omega_m^2 W_m = 0 \qquad \text{(A.1-6)}$$

$$(EI \cdot W_n'')'' - m\omega_n^2 W_n = 0. \qquad \text{(A.1-7)}$$

Multiplying Eq. (A.1-6) by W_n and Eq. (A.1-7) by W_m and then integrating along the beam of length ℓ we obtain

$$\int_0^\ell (EI\, W_m'')''\, W_n\, dx = \omega_m^2 \int_0^\ell W_m\, W_n\, m\, dx \qquad \text{(A.1-8)}$$

$$\int_0^\ell (EI\, W_n'')''\, W_m\, dx = \omega_n^2 \int_0^\ell W_n\, W_m\, m\, dx. \qquad \text{(A.1-9)}$$

Subtraction yields

$$(\omega_m^2 - \omega_n^2) \int_0^\ell W_m W_n\, m\, dx = \int_0^\ell [(EI\, W_m'')''\, W_n - (EI\, W_n'')''\, W_m]\, dx. \qquad \text{(A.1-10)}$$

After successive integrations by parts on the right side of Eq. (A.1-10) we obtain

80

$$(\omega_m^2 - \omega_n^2) \int_0^\ell W_m \, W_n \, m \, dx = \{ W_n \, (EI \cdot W_m'')' - W_m \, (EI \cdot W_n'')'$$

$$- EI \, (W_n' \, W_m'' - W_m' \, W_n'') \} \Big|_0^\ell. \qquad \text{(A.1-11)}$$

If at least one of the following pairs of boundary conditions holds, then the right side of Eq. (A.1-11) vanishes identically and the orthogonality condition is satisfied:

$$W = 0 \quad \text{and} \quad W' = 0 \qquad\qquad \text{(A.1-11a)}$$

$$W = 0 \quad \text{and} \quad EI \cdot W'' = 0 \qquad\qquad \text{(A.1-11b)}$$

$$W' = 0 \quad \text{and} \quad (EI \cdot W'')' = 0 \qquad\qquad \text{(A.1-11c)}$$

$$EI \cdot W'' = 0 \quad \text{and} \quad (EI \cdot W'')' = 0. \qquad\qquad \text{(A.1-11d)}$$

At this point, ready to tackle the solutions of Eqs. (A.1-4) and (A.1-5) we shall confine ourselves to uniform beams, hence EI and m are both assumed constant. Letting $a^2 = EI/m$, the aforementioned solutions are easily written by inspection

$$T = A \sin\omega t + B \cos\omega t \qquad\qquad \text{(A.1-12)}$$

$$W = C \sinh \sqrt{\tfrac{\omega}{a}}x + D \cosh \sqrt{\tfrac{\omega}{a}}x + E \sin \sqrt{\tfrac{\omega}{a}}x + F \cos\sqrt{\tfrac{\omega}{a}}x. \qquad \text{(A.1-13)}$$

where the constants A,B,C,D,E,F are determined by the boundary conditions.

For this investigation, we are interested in unrestrained beams, hence the natural boundary conditions are that moments and their derivatives with respect to position (shear) vanish at the end points. Thus

$$W''(0) = W'''(0) = W''(\ell) = W'''(\ell) = 0. \qquad\qquad \text{(A.1-14)}$$

Applying these boundary conditions to Eq. (A.1-13) we obtain

$$C = E, \qquad D = F \qquad\qquad \text{(A.1-15)}$$

$$(\sinh q\ell - \sin q\ell)C + (\cosh q\ell - \cos q\ell)D = 0$$

$$(\cosh q\ell - \cos q\ell)C + (\sinh q\ell - \sin q\ell)D = 0 \qquad (A.1-16)$$

where $q = \sqrt{\frac{\omega}{a}}$. Eq. (A.1-16) is a set of linear equations in C and D which will have a non-trivial solution only if the matrix of coefficients is of less than full rank. This requirement yields the following equation in ω, from which the eigenvalues or natural frequencies of vibration can be ascertained:

$$\cos\sqrt{\frac{\omega}{a}}\ell = \left(\cosh\sqrt{\frac{\omega}{a}}\ell\right)^{-1}. \qquad (A.1-17)$$

Solutions to Eq. (A.1-17) are of the form

$$\omega_n = \begin{cases} 0 & \text{for } n=0 \\ (1.51^2 \ (\frac{\pi}{\ell})^2 \ EI/m & \text{for } n=1 \\ \frac{2n+1}{2}^2 \ (\frac{\pi}{\ell})^2 \ EI/m & \text{for } n=2,3,\ldots \end{cases} \qquad (A.1-18)$$

and the eigenfunctions or normal mode shapes become

$$W_n(x) = G \left(\frac{\cos q_n\ell - \cosh q_n\ell}{\sinh q_n\ell - \sin q_n\ell}\right)(\sinh q_n x + \sin q_n x)$$

$$+ (\cosh q_n x + \cos q_n x) \qquad (A.1-19)$$

where $q_n = \sqrt{\frac{\omega_n}{a}}$ and G is an arbitrary scaling factor. $W_n(x)$ has been plotted for n=1,2 in Figure 3.

It will be advantageous for us to normalize the mode shapes. One widely used scheme defines

$$\phi_n(x) = B_n W_n(x) \qquad (A.1-20)$$

82

where the normalizing constant B_n satisfies

$$B_n^2 = \frac{M}{\int_0^{\ell} w_n^2(x) m \, dx} \qquad \text{(A.1-21)}$$

and M is the mass of the beam. Also define M_j, the generalized mass of the jth mode as

$$M_j = \int_0^{\ell} \phi_j^2(x) m \, dx \; . \qquad \text{(A.1-22)}$$

Note that for the normalization according to Eq. (A.1-20)

$$M_j = M \qquad \text{for all j} \; . \qquad \text{(A.1-23)}$$

With these additional mathematical tools in hand, we are ready to proceed to the matter of interest -- forced motion of the airframe. In this situation Eq. (A.1-1) becomes

$$(EIw''(x,t))'' + m\ddot{w}(x,t) = F_z(x,t) \; . \qquad \text{(A.1-24)}$$

As the normal mode shapes and natural frequencies have already been calculated, we can postulate the solution as

$$w(x,t) = \sum_{n=1}^{\infty} \phi_n(x) \, \xi_n(t) \qquad \text{(A.1-25)}$$

where the $\xi_n(t)$ are called normal coordinates and remain to be determined. Substituting Eq. (A.1-25) into Eq. (A.1-24) yields

$$m \sum_{n=1}^{\infty} \phi_n \ddot{\xi}_n + \sum_{n=1}^{\infty} (EI\phi_n'')'' \, \xi_n = F_z(x,t) \; . \qquad \text{(A.1-26)}$$

Multiplying by ϕ_m, integrating over the length of the beam, and using Eq. (A.1-8), we arrive at

$$\sum_{n=1}^{\infty} \ddot{\xi}_n \int_0^{\ell} \phi_n \phi_m \, mdx + \sum_{n=1}^{\infty} \xi_n \omega_n^2 \int_0^{\ell} \phi_n \phi_m \, mdx = \int_0^{\ell} F_z(x,t) \phi_m dx$$

(A.1-27)

where the order of the integral and summation operators has been inter-changed. However the ϕ_n's are mutually orthogonal with respect to the mass distribution, hence Eq. (A.1-27) simplifies to

$$\ddot{\xi}_m + \omega_m^2 \xi_m = Z_m / M_m$$

(A.1-28)

where

$$Z_m = \int_0^{\ell} F_z(x,t) \phi_m(x) \, dx .$$

(A.1-29)

If F_z is a point force of magnitude $F_z(t)$ concentrated at $x = x_0$, then we can write

$$F_z(x,t) = F_z(t) \, \delta(x-x_0)$$

(A.1-30)

and Eq. (A.1-28) further simplifies to

$$\ddot{\xi}_n + \omega_n^2 \xi_n = \phi_n(x_0) \cdot F_z(t) / M_n .$$

(A.1-31)

A.2. Integral Equations of Motion of a Slender Beam

For a restrained beam vibrating in the absence of external forces we can write

$$w(x,t) = -\int_{-\ell}^{\ell} C(x,\eta) \, \ddot{w}(\eta,t) \, m(\eta) \, d\eta,$$

(A.2-1)

84

where $C(x,\eta)$ is the conventional influence function measuring the displacement at x due to a unit force applied at r, with the origin of the x-axis constrained to its initial position. Since Eq. (A.2-1) is separable, it accepts a solution of the form

$$w(x,t) = W(x)\ T(t)\ .\qquad\qquad\text{(A.2-2)}$$

Substituting Eq. (A.2-2) into Eq. (A.2-1), remembering that x and t are independent variables, we obtain

$$\ddot{T} + \omega^2 T\ =\ 0\qquad\qquad\text{(A.2-3)}$$

$$W(x) = \omega^2 \int_{-\ell}^{\ell} C(x,\eta)\ W(\eta)\ m(\eta)\ d\eta.\qquad\text{(A.2-4)}$$

Note that Eq. (A.2-3) is identical to Eq. (A.1-4), and the family of solutions to Eq. (A.2-4) is identical to the solutions of Eq. (A.1-5) provided that the boundary conditions on Eq. (A.1-5) and $C(x,\eta)$ are the same.

Now, let us consider an unrestrained beam, as shown in Figure A1. The axes are chosen so that the origin coincides with the center of gravity of the beam, the x and z axes align with the principal inertial axes of the beam. Further, the beam is assumed symmetric with respect to the z-axis.

Since the beam vibrates freely, the sum of inertial forces in the z-direction and inertial moments about the y-axis are zero

$$\int_{-\ell}^{\ell} \ddot{w}(x,t)\ dm\ =\ \ddot{T}(t) \int_{-\ell}^{\ell} W(x)\ m(x)\ dx\ =\ 0\qquad\text{(A.2-5)}$$

$$\int_{-\ell}^{\ell} \ddot{w}(x,t)\ xdm\ =\ \ddot{T}(t) \int_{-\ell}^{\ell} W(x)\ m(x)\ xdx\ =\ 0.\qquad\text{(A.2-6)}$$
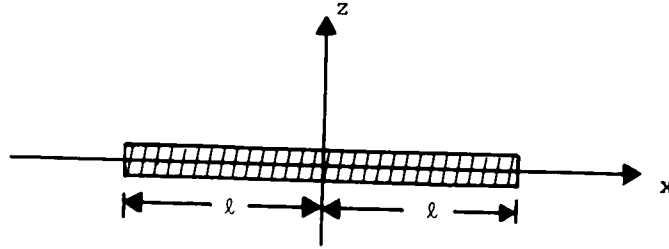
Figure Al. Beam with Coordinate Axes

If a unit load in the z-direction is applied at a point r along the beam, the resultant acceleration at a point x of the rigid beam is given by

$$a(x) = \frac{1}{M} + \frac{xr}{I_y} \qquad\qquad (A.2\text{-}7)$$

where M is the total mass of the beam and I_y is the moment of inertia about the y-axis. The inertial force due to an element of mass $m(x)\,dx$ is thence

$$df(x) = -\left(\frac{1}{M} + \frac{xr}{I_y}\right) m(x)\ dx \quad . \qquad\qquad (A.2\text{-}8)$$

The displacement of the flexible beam with respect to a line tangent to the beam at the origin, due to a unit force at the point r and the distributed inertial forces, can then be written

$$H(x,r) = C(x,r) - \int_{-\ell}^{\ell} C(x,\eta)\ \left(\frac{1}{M} + \frac{r}{I_y}\right) m(\eta)\ d\eta. \qquad (A.2\text{-}9)$$

86

(No attempt will be made to derive influence functions for the beam or aircraft. These can be calculated depending upon the physical properties of the structure involved. [See Ref. 1, Chapter 2] However, in this investigation, little insight into our problem will be garnered by pursuing the explicit characterization of the influence function.)

If beam deflection is measured with respect to the x-axis rather than a line parallel to it as in Eq. (A.2-9), then we can write a modified influence function

$$G(x,r) = H(x,r) + W(0) + \frac{\partial W(0)}{\partial x}^* x \qquad (A.2-10)$$

where the last two terms are simply the deflection and slope of the beam at the center of gravity. $G(x,r)$ in Eq. (A.2-10) represents a displacement of the beam, hence it must satisfy Eq. (A.2-5), yielding

$$\int_{-\ell}^{\ell} [H(x,r) + W(0) + \frac{\partial W(0)}{\partial x} x] \, m(x) \, dx = 0 \, . \qquad (A.2-11)$$

However as the origin is the center of gravity of the beam, Eq. (A.2-11) yields directly

$$W(0) = -\frac{1}{M} \int_{-\ell}^{\ell} H(x,r) \, m(x) \, dx \, . \qquad (A.2-12)$$

Similarly, substituting Eq. (A.2-11) into Eq. (A.2-6) and carrying out the indicated integration gives

$$\frac{\partial W(0)}{\partial x} = -\frac{1}{I_y} \int_{\ell}^{\ell} H(x,r) \, m(x) \, x dx \, . \qquad (A.2-13)$$

Having obtained explicit formulae for $W(0)$ and $\frac{\partial W(0)}{\partial x}$, we can now

---

* We will use this notation to designate the derivative evaluated at the point (0).

derive an expression for the influence function of an unrestrained beam with respect to its principal inertial axes

$$G(x,r) = C(x,r) - \int_{-\ell}^{\ell} C(x,\eta) \left(\frac{1}{M} + \frac{r\eta}{I_y}\right) m(\eta) \, d\eta$$

$$- \int_{-\ell}^{\ell} C(\eta,r) \left(\frac{1}{M} + \frac{x\eta}{I_y}\right) m(\eta) \, d\eta$$

$$+ \int_{\ell}^{\ell} \int_{-\ell}^{\ell} C(\rho,\eta) \left(\frac{1}{M} + \frac{r\eta + x\rho}{MI_y} + \frac{x\eta r\rho}{I_y^2}\right) m(\eta) m(\rho) \, d\rho \, d\xi.$$

$$(A.2-14)$$

Analogous to the situation for the restrained beam, Eq. (A.2-4), the integral equation for the freely vibrating unrestrained beam becomes

$$W(x) = \omega^2 \int_{\ell}^{\ell} G(x,r) \, W(r) \, m(r) \, dr. \qquad (A.2-15)$$

Further simplification in Eq. (A.2-15) is possible. From Eqs. (A.2-5) and (A.2-6) we see that any terms comprising $G(x,r)$ which include only zero or first powers of r will not contribute anything to the integral of Eq. (A.2-15). Examination of Eq. (A.2-13) shows that the second and fourth integrals have this property, and as a result, the influence function $G(x,r)$ can be simplified as follows:

$$G(x,r) = C(x,r) - \int_{-\ell}^{\ell} C(\eta,r) \left(\frac{1}{M} + \frac{x\eta}{I_y}\right) m(\eta) \, d\eta. \qquad (A.2-16)$$

Equation (A.21-5) in conjunction with Eq. (A.2-16) govern the natural vibration characteristics of the unrestrained slender beam. As was the case with the restrained beam, the family of solutions to Eq. (A.2-15) is identical to that via the differential equation analysis provided that $G(x,r)$ satisfies appropriate boundary conditions.

88

Having derived the influence function of the unrestrained beam, we can write the unrestrained beam analog of Eq. (2.2-1).

$$w(x,t) = -\int_{-\ell}^{\ell} G(x,r)\ddot{w}(r,t)m(r)dr. \qquad (A.2\text{-}17)$$

The extension to forced motion of the beam requires some care. Denoting the applied force per unit length in the z-direction as $F_z(x,t)$, one is tempted to write, for forced motion of the beam

$$w(x,t) = -\int_{-\ell}^{\ell} G(x,r)\ [-\ddot{w}(r,t)\ m(r) - F_z(r,t)]\ dr. \qquad (A.2\text{-}18)$$

However, the above is not correct. This is because the notion of the displacement function in the free and forced motion is different. In the former case, the displacement is measured with respect to the principal inertial axes of the beam. Equation (A.2-15) defines only elastic deformation modes of the beam. The effect of the integral term in Eq. (A.2-16) is to subtract off the effect of rigid body translations and rotation from the total motion of the beam. Thus Eq. (A.2-15) yields only trivial rigid body ($\omega = 0$) motion. For forced motion of the beam, the rigid body motion cannot be eliminated to leave the deformation modes alone. Thus, in this case, the displacement function, $w(x,t)$ must represent the total displacememt including translations, rotations, and elastic deformations.

The mode shapes generated by Eq. (A.2-15) are orthogonal with respect to the mass distribution, i.e.,

$$\int_{-\ell}^{\ell} W_n(x)\ W_m(x)\ m(x)\ dx\ =\ 0 \qquad (A.2\text{-}19)$$

for $m \neq n$. Proof of the orthogonality condition for the two dimensional case is given in Section 4. The proof of Eq. (A.2-19) is exactly the same and is not repeated here.

The analysis of the forced motion relies heavily on the concept of orthogonal mode shapes to represent the motion of the beam, and as in the differential equation derivation we assume a solution of the form

$$w(x,t) = \sum_{n=1}^{\infty} \phi_n(x) \; \xi_n(t).$$ (A.1-25)

Finally, the equations of forced motion are readily simplified to

$$M_j \ddot{\xi}(t) + M_j \omega_j^2 \xi_j(t) = \int_{-\ell}^{\ell} F_z(x,t) \; \phi_j(x) \; dx$$ (A.2-20)

where

$$M_j = \int_{-\ell}^{\ell} \phi_j^2(x) m(x) \; dx \; .$$ (A.2-21)

One mode relates the rigid body translation and another the rigid body rotation. Letting these be the first and second modes, their corresponding mode shapes are

$$\phi_1(x) = 1$$ (A.2-21)

$$\phi_2(x) = x.$$ (A.2-22)

The derivation of the analogue of Eq. (A.2-20) is given for the two dimensional case in Section 5. There is no difference in approach between the one and two dimensional situations, hence the proof of Eq. (A.2-20) is omitted here.

A.3. Free Vibration of the Unrestrained Aircraft

From Chapter 1, Section A.2, we have for the aircraft in the absence of external forces

90

$$\iint_S \ddot{w}(x,y,t) \; \rho(x,y) \; dxdy \;\; = \;\; 0 \tag{A.3-1}$$

$$\iint_S \ddot{w}(x,y,t) \; x\rho(x,y) \; dxdy \;\; = \;\; 0 \tag{A.3-2}$$

$$\iint_S \ddot{w}(x,y,t) y\rho(x,y) \; dxdy \;\; = \;\; 0 \;\; \cdot \tag{A.3-3}$$

In addition, the relation between inertial and elastic forces yields

$$w(x,y,t) \; - \; w(0,0,t) \; - \; x \; \frac{\partial w(0,0,t)}{\partial x} \; - \; y \; \frac{\partial w(0,0,t)}{\partial y}$$

$$= \; - \iint_S C(x,y;\xi,\eta)\rho(\xi,\eta)\ddot{w} \; (\xi,\eta,t) \; d\xi d\eta. \tag{A.3-4}$$

Upon imposition of a solution of the form

$$w(x,y,t) \; = \; W(x,y)T(t) \tag{A.3-5}$$

the four equations of motion become

$$\iint_S W(x,y)\rho(x,y) \; dxdy \;\; = \;\; 0 \tag{A.3-6}$$

$$\iint_S W(x,y) \; x\rho(x,y) \; dxdy \; = \;\; 0 \tag{A.3-7}$$

$$\iint_S W(x,y) \; y\rho(x,y) \; dxdy \; = \;\; 0 \tag{A.3.8}$$

$$T \; [W(x,y) \; - \; W(0,0) \; - \; x\frac{\partial W(0,0)}{\partial x} \; - \; y\frac{\partial W(0,0)}{\partial y}]$$

$$= \; -\ddot{T}\iint_S C(x,y;\xi,\eta) \; \rho(\xi,\eta) \; W(\xi,\eta) \; d\xi d\eta. \tag{A.3-9}$$

Note that Eq. (A.3-9) is separable and reduces to

$$\ddot{T} \; +\omega^2 T \; = \;\; 0 \tag{A.3-10}$$

$$W(x,y) - W(0,0) - x \frac{\partial W(0,0)}{\partial x} - y \frac{\partial W(0,0)}{\partial y}$$

$$= \omega^2 \iint_S C(x,y;\xi,\eta) \rho(\xi,\eta) W(\xi,\eta) d\xi d\eta \qquad (A.3-11)$$

where ω^2 is a constant of proportionality of dimension $\sec^{-2}$.

As was the case in the one dimensional beam theory, we shall be able to eliminate the terms representing the amplitude and deflection at the center of gravity. Multiplying Eq. (A.3-11) by $\rho(x,y)$ and then integrating over the surface of the airplane, we obtain

$$\iint_S W(x,y) \rho(x,y) \, dxdy - W(0,0) \iint_S \rho(x,y) \, dxdy$$

$$- \frac{\partial W(0,0)}{\partial x} \iint_S x\rho(x,y) \, dxdy - \frac{\partial W(0,0)}{\partial y} \iint_S y\rho(x,y) \, dxdy$$

$$= \omega^2 \iint_S \rho(x,y) \iint_S C(x,y;\xi,\eta) \, \rho(\xi,\eta) \, W(\xi,\eta) \, d\xi d\eta dxdy.$$

$$(A.3.12)$$

But the first integral vanishes by Eq. (A.3-6) and the third and fourth integrals likewise vanish by the definition of center of gravity. Hence Eq. (A.3-12) may be solved for $W(0,0)$ as follows:

$$W(0,0) = - \frac{\omega^2}{M} \iint_S \rho(x,y) \iint_S C(x,y;\xi,\eta) \rho(\xi,\eta) \, W(\xi,\eta) d\xi d\eta dxdy$$

$$(A.3-13)$$

where M is the mass of the aircraft.

Returning to Eq. (A.3-11), multiplying by $x\rho(x,y)$ followed by integration over the surface yields

$$\frac{\partial W(0,0)}{\partial x} = - \frac{\omega^2}{I_y} \iint_S x\rho(x,y) \iint_S C(x,y;\xi,\eta) \rho(\xi,\eta) \, W(\xi,\eta) d\xi d\eta dxdy$$

where

$$(A.3-14)$$

$$I_y = \iint_S x^2 \rho(x,y) dxdy. \qquad (A.3-15)$$

Similarly, multiplication of Eq. (A.3-11) by $y\rho(x,y)$ and subsequent integration leads to

$$\frac{\partial W(0,0)}{\partial y} = -\frac{\omega^2}{I_x} \iint_S y\rho(x,y) \iint_S C(x,y;\xi,\eta)\,\rho(\xi,\eta)W(\xi,\eta)\,d\xi d\eta dxdy$$

(A.3-16)

where

$$I_x = \iint_S y^2\rho(x,y)\,dxdy.$$

(A.3-17)

Substituting Eqs. (A.3-13), (A.3-14) and (A.3-16) into Eq. (A.3-11) we obtain the integral equation governing the mode shapes of the free vibration of the aircraft

$$W(x,y) = \omega^2 \iint_S G(x,y;\xi,\eta)W(\xi,\eta)\,\rho(\xi,\eta)d\xi d\eta$$

(A.3-18)

where

$$G(x,y;\xi,\eta) = C(x,y;\xi,\eta) - \iint_S C(r,s;\xi,\eta)\left[\frac{1}{M}+\frac{xr}{I_y}+\frac{ys}{I_x}\right]\rho(r,s)drds.$$

(A.3-19)

A.4. Orthogonality Condition for Mode Shapes

The mode shapes of the unrestrained aircraft can be shown orthogonal as follows. For any two different modes we can write, from Eq. (A.3-18)

$$W_n(x,y) = \omega_n^2 \iint_S G(x,y;\xi,\eta)W_n(\xi,\eta)\rho(\xi,\eta)\,d\xi d\eta$$

(A.4-1)

$$W_m(x,y) = \omega_m^2 \iint_S G(x,y;\xi,\eta)\,W_m(\xi,\eta)\rho(\xi,\eta)d\xi d\eta.$$

(A.4-2)

Multiplying Eqs. (A.4-1) and (A.4-2) by $W_m(x,y)\rho(x,y)$ and $W_n(x,y)\rho(x,y)$ respectively and integrating over the surface of the airplane, we obtain

$$\frac{1}{\omega_n^2}\iint_S W_n W_m \ \rho dxdy = \iint_S W_m \rho \left[\iint_S GW_n \rho d\xi d\eta\right] dxdy \qquad (A.4-3)$$

$$\frac{1}{\omega_m^2}\iint_S W_m W_n \rho dxdy = \iint_S W_n \rho \left[\iint_S GW_m \rho d\xi d\eta dxdy\right]. \qquad (A.4-4)$$

By interchanging the dummy arguments and then reversing the order of integration, the right side of Eq. (A.4-4) becomes

$$\frac{1}{\omega_m^2}\iint_S W_m W_n \ \rho dxdy$$

$$= \iint_S W_m(x,y)\rho(x,y)\left[\iint_S G(\xi,\eta;x,y)\ W_n(\xi,\eta)\rho(\xi,\eta)\ d\xi d\eta\right] dxdy.$$

$$(A.4-5)$$

In Section 3 the influence function for the unrestrained airplane was derived

$$G(x,y;\xi,\eta) = C(x,y;\xi,\eta) - \iint_S C(r,s;\xi,\eta)\left[\frac{1}{M} + \frac{xr}{I_y} + \frac{ys}{I_x}\right]\rho(r,s)drds \ .$$

$$(A.3-17)$$

Noting that $C(x,y;\xi,\eta) = C(\xi,\eta;x,y)$, [See Ref.1, Chapter 2] it is obvious from Eq. (A.3-17) that

$$G(\xi,\eta;x,y) = G(x,y;\xi,\eta) + \iint_S C(r,s;\xi,\eta)\left[\frac{1}{M} + \frac{xr}{I_y} + \frac{ys}{I_x}\right]\rho(r,s)drds.$$

$$-\iint_S C(r,s;x,y)\left[\frac{1}{M} + \frac{\xi r}{I_y} + \frac{\eta s}{I_x}\right]\rho(r,s)drds. \qquad (A.4-6)$$

94

Substituting Eq. (A.4-6) into Eq. (A.4-5) we arrive at

$$\frac{1}{\omega_m^2} \iint_S W_m W_n \rho dx dy = \iint_S W_m(x,y)\, \rho(x,y) \left\{ \iint_S [G(x,y;\xi,\eta) \right.$$

$$+ \iint_S C(r,s;\xi,\eta) \left[\frac{1}{M} + \frac{xr}{I_y} + \frac{ys}{I_x} \right] \rho(r,s)\ drds$$

$$- \iint_S C(r,s;x,y) \left[\frac{1}{M} + \frac{\xi r}{I_y} + \frac{\eta s}{I_x} \right] \rho(r,s)\ drds \Bigg]$$

$$\left. \cdot W_n(\xi,\eta)\, \rho(\xi,\eta)\ d\xi d\eta \right\}\ dx dy. \qquad (A.4-7)$$

Upon expanding Eq. (A.4-7) into the sum of three integrals, it is immediately clear that the third integral vanishes by application of Eqs. (A.3-1), (A.3-2) and (A.3-3), as both ξ and η appear to the zero or first power in the inner integral. If we interchange the order of integration in the second integral, performing the integration with respect to x and y first, then a similar situation occurs, and by Eqs. (A.3-1), (A.3-2), and (A.3-3) again, the second integral will contribute nothing. Whence Eq. (A.4-7) simplifies to

$$\frac{1}{\omega_m^2} \iint_S W_m W_n\ \rho dx dy = \iint_S W_m \left[\iint_S G W_n \rho d\xi d\eta \right] dx dy. \qquad (A.4-8)$$

Comparison with Eq. (A.4-3) immediately reveals

$$\left(\frac{1}{\omega_n^2} - \frac{1}{\omega_m^2} \right) \iint_S W_m W_n\ \rho dx dy = 0 \qquad (A.4-9)$$

which for $m \neq n$ is the desired orthogonality condition.

Furthermore, the mode shapes corresponding to the rigid translation and rotation of the unrestrained aircraft under external forces, given by Eqs. (1-15) and (1-16) respectively, are also orthogonal to all the deformation mode shapes and each other. This is an immediate consequence of Eqs. (1-1) and (1-2) and the definition of the center of gravity.

A.5   Forced Motion of the Unrestrained Aircraft

From Chapter 1, by equilibrium of forces and moments, we have

$$\iint_S \ddot{w}(x,y,t) \; \rho(x,y) \; dxdy = \iint_S F_z(x,y,t) \; dxdy \tag{A.5-1}$$

$$\iint_S \ddot{w}(x,y,t) x\rho(x,y) \; dxdy = \iint_S F_z(x,y,t) xdxdy \tag{A.5-2}$$

and relating inertial and elastic forces we obtain

$$w(x,y,t) - w(0,0,t) - x\frac{\partial w(0,0,t)}{\partial x}$$

$$= \iint_S C(x,y;r,s)\left[F_z(r,s,t) - \ddot{w}(r,s,t)\rho(r,s)\right] drds. \tag{A.5-3}$$

Assuming a solution of the form analogous to that for motion of the one dimensional beam,

$$W(x,y,t) = \sum_{n=1}^{\infty} \phi_n(x,y) \; \xi_n(t). \tag{A.5-4}$$

The rigid body motion can be characterized by the modes

$$\phi_1(x,y) = 1 \qquad \omega_1 = 0 \tag{A.5-5}$$

$$\phi_2(x,y) = x \qquad \omega_2 = 0. \tag{A.5-6}$$

The other modes represent the elastic deformation with respect to the inertial plane of the aircraft, and hence from Eq. (A.3-11) we have

$$\phi_n(x,y) - \phi_n(0,0) - x\frac{\partial\phi_n(0,0)}{\partial x}$$

$$= \omega_n^2 \iint_S C(x,y;r,s)\rho(r,s)\phi_n(r,s) \, drds \qquad (A.5-7)$$

with the additional constraints from Eqs. (A.3-7) and (A.3-8)

$$\iint_S \phi_n(x,y)\rho(x,y) \, dxdy = 0 \qquad (A.5-8)$$

$$\iint_S \phi_n(x,y)x\rho(x,y) \, dxdy = 0 \ . \qquad (A.5-9)$$

The substitution of Eq. (A.5-4) into Eq. (A.5-1) in conjunction with Eqs. (A.5-5) and (A.5-8) yields simply

$$\ddot{\xi}_1 \iint_S \rho(x,y) \, dxdy = M_1\ddot{\xi}_1 = \iint_S F_z(x,y,t) \, dxdy. \qquad (A.5-10)$$

Similarly, substitution of Eq. (A.5-4) into Eq. (A.5-2) together with Eqs. (A.5-6) and (A.5-9) gives

$$\ddot{\xi}_2 \iint_S x^2\rho(x,y) \, dxdy = M_2\ddot{\xi}_2 = \iint_S F_z(x,y,t) \, xdxdy. \qquad (A.5-11)$$

Note that M_1 and M_2 are the mass and pitching moment of inertia respectively.

If we now introduce Eq. (A.5-4) into Eq. (A.5-3) we obtain

$$\sum_{n=1}^{\infty} \left[\phi_n(x,y) - \phi_n(0,0) - x\frac{\partial \phi_n(0,0)}{\partial x} \right] \xi_n(t)$$

$$= \iint_S C(x,y;r,s) \left[F_z(r,s,t) - \rho(r,s) \sum_{n=1}^{\infty} \phi_n(r,s) \ddot{\xi}_n(t) \right] drds.$$

$$(A.5-12)$$

Noting that

$$\phi_j(x,y) - \phi_j(0,0) - x\frac{\partial \phi_n(0,0)}{\partial x} = 0 \qquad (A.5-13)$$

for j=1 and 2, and applying Eq. (A.5-7) we can rewrite Eq. (A.5-12)

$$\sum_{n=3}^{\infty} \left[\phi_n(x,y) - \phi_n(0,0) - x\frac{\partial \phi_n(0,0)}{\partial x} \right] \left(\xi_n(t) + \frac{\ddot{\xi}_n(t)}{\omega_n^2} \right)$$

$$= \iint_S C(x,y;r,s) \left[F_z(r,s,t) - \rho(r,s)(\ddot{\xi}_1(t) + r\ddot{\xi}_2(t)) \right] drds.$$

$$(A.5-14)$$

Multiplying by $\phi_m(x,y) \rho(x,y)$ and integrating over the surface yields, after the application of Eqs. (A.5-8) and (A.5-9) and the orthogonality condition of the mode shapes,

$$M_m \left(\frac{\ddot{\xi}_m}{\omega_m^2} + \xi_m \right) = \iint_S \phi_m(x,y) \rho(x,y) \iint_S C(x,y;r,s) \cdot$$

$$\left[F_z(r,s,t) - \rho(r,s)(\ddot{\xi}_1 + r\ddot{\xi}_2) \right] drds. \qquad (A.5-15)$$

As the influence function is symmetric, [See Ref. 1, Chapter 2]

$$C(x,y;r,s) = C(r,s;x,y) \qquad (A.5-16)$$

98

we can interchange the variables of integration and the order of integration in Equation (A.5-15) to achieve

$$M_m\left(\frac{\ddot{\xi}_m}{\omega_m^2} + \ddot{\xi}_m\right) = \iint_S \left[F_z(x,y,t) - \rho(x,y)\,(\ddot{\xi}_1 + x\ddot{\xi}_2) \right]$$

$$\cdot \iint_S C(x,y;r,s)\,\phi_m(r,s)\,\rho(r,s)\ drdsdxdy. \qquad (A.5-17)$$

The use of Eq. (A.5-7) allows us to simplify the right side of Eq. (A.5-17) even further

$$M_m\left(\frac{\ddot{\xi}_m}{\omega_m^2} + \xi_m\right) = \frac{1}{\omega_m^2} \iint_S \left[F_z(x,y,t) - \rho(x,y)\,(\ddot{\xi}_1 + x\ddot{\xi}_2) \right] \cdot$$

$$\left[\phi_m(x,y) - \phi_m(0,0) - x\frac{\partial\phi_m(0,0)}{\partial x} \right] dxdy. \qquad (A.5-18)$$

Expanding the right side of above and making use of Eqs. (A.5-8), (A.5-9), (A.5-10) and (A.5-11), together with the definition of center of mass, Eq. (A.5-18) reduces considerably to

$$M_m\ddot{\xi}_m + \omega_m^2\xi_m = \iint_S F_z(x,y,t)\ \phi_m(x,y)\ dxdy. \qquad (A.5-19)$$

Although the derivation of Eq. (A.5-19) was restricted to the elastic deformation modes, Eqs. (A.5-10) and (A.5-11) show that the rigid body motion can be similarly represented.

APPENDIX B

Rigid Body Motion - Longitudinal Group

For this analysis, we will assume the aircraft is in an equilibrium constant altitude flight condition. We choose the coordinate system as follows: the x-axis coincides with the equilibrium direction of flight, the z-axis is chosen down, and the y-axis is taken out the wing to form a right handed coordinate system. As usual, the origin is at the airplane center of gravity. Once set, the axes are fixed to the airplane, and rotate along with the aircraft.
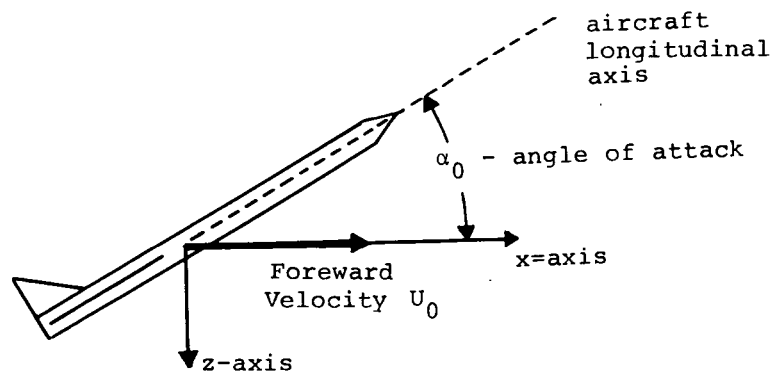
Figure B1. Airplane in Equilibrium Flight Condition

Following Figure B1, we will denote the aircraft forward velocity by

$$U = U_0 + u \qquad \qquad (B-1)$$

where u represents the velocity perturbation along the x-axis. The velocity along the z-axis is given by

$$W = U_0 \alpha \qquad\qquad (B-2)$$

where α is the perturbation angle of attack. Note that a positive increment in α_0 without a rotation of the aircraft induces a positive z-component of velocity. We let θ represent the rotation in inertial space of the airframe about the y-axis. Thus θ, the pitch angle, measures the rotation of the x-axis from its initial alignment. Finally, the deviation from nominal altitude is given by h.

With the mass and pitching moment of inertia designated by m and I_y respectively, we can write the linearized inertial equations of motion

$$\delta X = m U_0 \frac{d}{dt} \left(\frac{u}{U_0}\right) \qquad\qquad (B-3)$$

$$\delta Z = m U_0 \left(\frac{d\alpha}{dt} - \frac{d\theta}{dt}\right) \qquad\qquad (B-4)$$

$$\delta P = I_y \frac{d^2\theta}{dt^2} \qquad\qquad (B-5)$$

where X and Z denote the forces along the x and z-axes, and P is the pitching moment. The first order perturbations in gravity forces due to a rotation of the aircraft are given by

$$\delta X_g = -mg \qquad\qquad (B-6)$$

$$\delta Z_g = 0. \qquad\qquad (B-7)$$

Following the usual convention, the aerodynamic forces and moments are normalized as below:

102

$$X_a = \frac{1}{2} \rho U_0^2 SC_x \tag{B-8}$$

$$Z_a = \frac{1}{2} \rho U_0^2 SC_z \tag{B-9}$$

$$P_a = \frac{1}{2} \rho U_0^2 ScC_m \tag{B-10}$$

where ρ is the atmospheric density, S is the aircraft lifting surface area, and c is the reference wing chord length. The term $\frac{1}{2} \rho U_0^2$ is called the dynamic pressure, and will henceforth be designated by q.

Two other fundamental parameters for any aircraft analysis are the coefficients of lift and drag, C_L and C_D. The lift coefficient is readily calculated by

$$C_L = \frac{mg}{qS}. \tag{B-11}$$

For supersonic flight, the following approximation is quite accurate

$$C_L = \frac{4\alpha_0}{(M^2 - 1)^{\frac{1}{2}}} \tag{B-12}$$

where M is the Mach number, and allows for a calculation of the equilibrium angle of attack. Again, for supersonic flight, we can approximate the drag coefficient by

$$C_D = C_{D_0} + \frac{(M^2-1)^{\frac{1}{2}}}{4} C_L^2 = C_{D_0} + \frac{\partial C_D}{\partial (C_L^2)} C_L^2 \tag{B-13}$$

where C_{D_0} is the skin friction component of drag.

The normalized forces and moment, obviously zero at equilibrium, are functions of the flight variables, U_0, α_0, h_0, pitch angle, and elevator deflection angle. For small perturbations in these quantities, we can write, to first order,

$$C_x = C_{x_u} \frac{u}{U_0} + C_{x_\alpha} \alpha \tag{B-14}$$

$$C_z = C_{z_u} \frac{u}{U_0} + C_{z_\alpha} \alpha + C_{z_\delta} \delta - C_{z_\rho} \frac{h}{h_0} \tag{B-15}$$

$$C_m = C_{m_u} \frac{u}{U_0} + \frac{c}{2U_0} C_{m_{\dot\alpha}} \dot\alpha + C_{m_\alpha} \alpha + \frac{c}{2U_0} C_{m_{\dot\theta}} \dot\theta + C_{m_\delta} \delta \tag{B-16}$$

where δ is the perturbation elevator deflection angle. The coefficients on the right side above are stability derivatives, partial derivatives of the forces and moments with respect to equation variables.

The term C_{x_u} is the speed damping derivative as it relates the resistance due to a change in forward speed. For jet aircraft, we can use the approximation

$$C_{x_u} = \frac{\partial C_x}{\partial \left(\frac{u}{U_0}\right)} = -\left(2C_D + \frac{\partial C_D}{\partial P} M\right). \tag{B-17}$$

Similarly, the term C_{z_u} reflects the lift due to an increase in speed

$$C_{z_u} = \frac{\partial C_z}{\partial \left(\frac{u}{U_0}\right)} = -\left(2C_L + \frac{\partial C_L}{\partial P} M\right). \tag{B-18}$$

The derivative C_{m_u} is defined as

$$C_{m_u} = \frac{\partial C_m}{\partial \left(\frac{u}{U_0}\right)} = \frac{\partial C_m}{\partial P} M \tag{B-19}$$

104

and relates changes in pitching moment to an increase of speed. It is primarily due to the center of pressure moving aftward with an increase of speed in the transonic region. For high Mach number flight, this derivative is negligible, as are the $\frac{\partial C_D}{\partial P}$ and $\frac{\partial C_L}{\partial P}$ terms.

The α derivatives relate changes in the resultant forces and moment induced by an increase in angle of attack,

$$C_{x_\alpha} = \frac{\partial C_x}{\partial \alpha} = C_L \left[1 - 2\frac{dC_D}{d(C_L^2)} \frac{\partial C_L}{\partial \alpha} \right]. \tag{B-20}$$

For supersonic flight however,

$$\frac{dC_D}{d(C_L^2)} = \frac{1}{\frac{\partial C_L}{\partial \alpha}} = \frac{(M^2 - 1)^{\frac{1}{2}}}{4} \tag{B-21}$$

so that Eq. (B-21) simplifies to

$$C_{x_\alpha} = -C_L. \tag{B-22}$$

The C_{z_α} term is given by

$$C_{z_\alpha} = \frac{\partial C_z}{\partial \alpha} = -(\frac{\partial C_L}{\partial \alpha} + C_D). \tag{B-23}$$

The stability derivative C_{m_α} relates changes in pitching moment due to the change in aerodynamic center of pressure effected by a perturbation in angle of attack. This term is negative for a stable aircraft, lest the effect of a small change in angle of attack is to induce a motion driving the airplane further from its equilibrium state,

$$C_{m_\alpha} = \frac{\partial C_m}{\partial \alpha} = \frac{\partial C_m}{\partial C_L} \frac{\partial C_L}{\partial \alpha}. \qquad \text{(B-24)}$$

The value of C_{m_α} decreases in magnitude as the center of gravity moves aft, and for the B-2707 prototype is approximately -0.2.

The derivative $C_{m_{\dot\theta}}$ is called the damping in pitch, and represents the aerodynamic effects that accompany a rotation of the airplane in the xz-plane;

$$C_{m_{\dot\theta}} = \frac{\partial C_m}{\partial (\frac{c}{2U_0}\dot\theta)}. \qquad \text{(B-25)}$$

This term is primarily due to the effect of the tail, and for the SST model is approximately -3.

The $\dot\alpha$ derivative $C_{m_{\dot\alpha}}$ arises since given a change in α, the pressure distribution over the lifting surfaces does not adjust instantaneously to an equilibrium value. This term is very difficult to determine for the wings and body of the airplane as it involves unsteady flow. The effect of the tail is derived primarily from the concept of the lag of the downwash. The downwash angle, ε, measures the downward deflection of the airflow at the tail due to the influence of the wings. Letting l_T denote the distance from the center of gravity to the center of the tail, and S_T the surface area of the tail, we can write

$$C_{M_{\dot\alpha}} = \frac{\partial C_m}{\partial (\frac{c}{2U_0}\dot\alpha)} \qquad \text{(B-26)}$$

$$(C_{m_{\dot\alpha}})_T = -2(\frac{l_T}{c})^2 \frac{S_T}{S} (\frac{\partial C_L}{\partial \alpha})_T \frac{\partial \varepsilon}{\partial \alpha}. \qquad \text{(B-27)}$$

In the swept-wing configuration of the B-2702, the $C_{m_{\dot{\alpha}}}$ term is negligible.

The derivative C_{z_ρ} denotes changes in the force along the z-axis due to an increase in altitude, and is given by

$$C_{z_\rho} = \frac{\partial C_z}{\partial(\frac{\partial \rho}{\rho})} = -C_L . \qquad \text{(B-28)}$$

The δ derivatives relate changes in forces and moments with respect to elevator deflections. In the swept-wing configuration, and elevator deflection (measured positive downward) has the effect of changing the angle of attack for a portion of the lifting surface. This creates a force equal to that supplied by a lifting surface of area the same as the elevator. Thus

$$C_{z_\delta} = \frac{\partial C_z}{\partial \delta} = -\frac{S_E}{S} \frac{\partial C_L}{\partial \alpha} \qquad \text{(B-29)}$$

where S_E is the area of the elevator. Similarly,

$$C_{m_\delta} = \frac{\partial C_m}{\partial \delta} = -\frac{l_E S_E}{cS} \frac{\partial C_L}{\partial \alpha} \qquad \text{(B-30)}$$

where l_E is the distance from the center of gravity to the elevator.

As the aircraft is unrestrained, the sum of the aerodynamic and gravitational forces must be in equilibrium with the inertial acceleration. From Eqs. (B-3) through (B-10) and (B-14) through (B-16) we obtain the equations of motion:

$$\frac{mU_0}{qS} \frac{\dot{u}}{U_0} - C_{x_u} \frac{u}{U_0} - C_{x_\alpha} \alpha + \frac{mg}{qS} \theta = 0 \qquad \text{(B-31)}$$

$$-C_{z_u}\frac{u}{U_0} + \frac{mU_0}{qS}\dot{\alpha} - C_{z_\alpha}\alpha - \frac{mU_0}{qS}\dot{\theta} + C_{z_\rho}\frac{h}{h_0} = C_{z_\delta}\delta \qquad (B-32)$$

$$C_{m_u}\frac{u}{U_0} - \frac{c}{2U_0}C_{m_{\dot\alpha}}\dot{\alpha} - C_{m_\alpha}\alpha + \frac{I_y}{qSc}\ddot{\theta} - \frac{c}{2U_0}C_{m_{\dot\theta}}\dot{\theta} = C_{m_\delta}\delta \;. \qquad (B-33)$$

In addition, a single integration of Eq. (B-4) yields

$$\frac{U_0}{h_0}\alpha - \frac{U_0}{h_0}\theta + \frac{\dot{h}}{h_0} = 0 . \qquad (B-34)$$

The four equations above are called the airplane longitudinal group and are most often presented in the form below, where D stands for the differentiation operator with respect to time:

$$\begin{bmatrix} \frac{mU_0}{qS}D - C_{x_u} & -C_{x_\alpha} & \frac{mg}{qS} & 0 \\[2em] -C_{z_u} & \frac{mU_0}{qS}D - C_{z_\alpha} & -\frac{mU_0}{qS}D & C_{z_\rho} \\[2em] -C_{m_u} & -\left(\frac{c}{2U_0}C_{m_{\dot\alpha}}D + C_{m_\alpha}\right) & \frac{I_y}{qSc}D^2 - \frac{c}{2U_0}C_{m_{\dot\theta}}D & 0 \\[2em] 0 & \frac{U_0}{h_0} & -\frac{U_0}{h_0} & D \end{bmatrix} \begin{bmatrix} \frac{u}{U_0} \\[1em] \alpha \\[1em] \theta \\[1em] \frac{h}{h_0} \end{bmatrix} = \begin{bmatrix} 0 \\[1em] C_{z_\delta} \\[1em] C_{m_\delta} \\[1em] 0 \end{bmatrix}\delta .$$

$$(B-35)$$

Eq. (B-35) can be put in the form of a minimum realization linear dynamical system as follows:

$$\underline{\dot{x}}_1 \;=\; \underline{A}_1 \underline{x}_1 + \underline{B}_1 u_1 \qquad\qquad (B\text{-}36)$$

where

$$\underline{x}_1' \;=\; [\; u \quad \alpha \quad \theta \quad \dot{\theta} \quad h \;]. \qquad\qquad (B\text{-}37)$$

$$
\underline{A}_1 =
\begin{bmatrix}
\dfrac{C_{\dot{x}_u}}{U_0}\Big/\dfrac{m}{qS} & C_{x_\alpha}\Big/\dfrac{m}{qS} & -g & 0 & 0 \\[2em]
C_{z_u}\Big/\dfrac{mU_0}{qS} & C_{z_\alpha}\Big/\dfrac{mU_0}{qS} & 0 & 1 & \dfrac{C_{z_\rho}}{h_0}\Big/\dfrac{mU_0}{qS} \\[2em]
0 & 0 & 0 & 1 & 0 \\[2em]
\dfrac{qSc}{I_y}\!\left(\dfrac{C_{m_u}}{U_0} + \dfrac{c}{2U_0}C_{m_{\dot\alpha}}\dfrac{C_{z_u}}{U_0}\Big/\dfrac{mU_0}{qS}\right) & \dfrac{qSc}{I_y}\!\left(C_{m_\alpha} + \dfrac{c}{2U_0}C_{m_{\dot\alpha}}\,C_{z_\alpha}\Big/\dfrac{mU_0}{qS}\right) & 0 & \dfrac{qSc}{I_y}\dfrac{c}{2U_0}(C_{m_{\dot\theta}}+C_{m_{\dot\alpha}}) & \dfrac{qSc}{I_y}\!\left(\dfrac{c}{2U_0}C_{m_{\dot\alpha}}\dfrac{C_{z_\rho}}{h_0}\dfrac{mU_0}{qS}\right) \\[2em]
0 & -U_0 & U_0 & 0 & 0
\end{bmatrix}
\qquad (B\text{-}38)
$$

$$\underline{B}_1' = [\ 0 \quad C_{z_\delta}/\dfrac{mU_0}{qS} \quad 0 \quad \dfrac{qSc}{I_y}(C_{m_\delta} + \dfrac{c}{2U_0}C_{m_{\dot\alpha}}C_{z_\delta}/\dfrac{mU_0}{qS}) \quad 0\ ] \quad (B-39)$$

and the control

$$u_1 = \delta. \qquad (B-40)$$

APPENDIX C

Derivation of Feedback Control Gains

Consider the following time invariant linear system with quadratic cost criterion

$$\dot{\underline{x}}(t) = \underline{A}\underline{x}(t) + \underline{B}\underline{u}(t) \tag{C-1}$$

$$J = \underline{x}'(T)\underline{Q}\underline{x}(T) + \int_0^T [\underline{x}'(t) \quad \underline{u}'(t)] \begin{bmatrix} \underline{L} & \underline{N} \\ \underline{N}' & \underline{R} \end{bmatrix} \begin{bmatrix} \underline{x}(t) \\ \underline{u}(t) \end{bmatrix} dt. \tag{C-2}$$

We will show that the control u*(t), which minimized J subject to Eq. (C-1), exists, and that this control is a linear functional of the state. We shall restrict our model by assuming the following conditions on the matrices L, N, R, and Q:

$$L' = L \geq 0 \qquad \text{(non-negative definite)} \tag{C-3a}$$

$$Q' = Q \geq 0 \tag{C-3b}$$

$$R' = R > 0 \qquad \text{(positive definite)} \tag{C-3c}$$

$$L - NR^{-1}N' \geq 0. \tag{C-3d}$$

The symmetry and definiteness relations of Eq. (C-3) involve no real loss of generality as far as practical, real-world systems go. Any quadratic form $\underline{x}'\underline{S}\underline{x}$ can be put in the form

$$\underline{x}'\underline{S}\underline{x} = \underline{x}'\underline{S}_1\underline{x} \quad \text{where} \quad \underline{S}_1' = \underline{S}_1. \tag{C-4}$$

The definiteness relations guarantee that a minimum for J does exist

for all possible state trajectories and controls. Obviously, that minimum is zero.

First, we state and prove a simple lemma. For $\underline{x}$ and $\underline{u}$ related as in Eq. (C-1), and $\underline{K}(t)$ a matrix differentiable on $0,T$, then

$$\int_0^T [\underline{x}'(t) \quad \underline{u}'(t)] \begin{bmatrix} \dot{\underline{K}}(t)+\underline{K}(t)\underline{A}+\underline{A}'\underline{K}(t) & \underline{K}(t)\underline{B} \\ \underline{B}'\underline{K}(t) & \underline{0} \end{bmatrix} \begin{bmatrix} \underline{x}(t) \\ \underline{u}(t) \end{bmatrix} dt$$

$$- \underline{x}'(t)\underline{K}(t)\underline{x}(t) \Big|_0^T = 0. \qquad \text{(C-5)}$$

The proof of Eq. (D-5) is as follows: for any differentiable $\underline{x}$ and $\underline{K}$ we have

$$\int_0^T \frac{d}{dt} [\underline{x}'(t)\underline{K}(t)\underline{x}(t)] \, dt - \underline{x}'(t)\underline{K}(t)\underline{x}(t) \Big|_0^T = 0. \qquad \text{(C-6)}$$

Eq. (C-6) can be rewritten

$$\int_0^T [\underline{x}'(t)\underline{K}(t)\underline{x}(t) + \underline{x}'(t)\underline{K}(t)\underline{x}(T) + \underline{x}'(t)\underline{K}(t)\underline{x}(t)] \, dt$$

$$- \underline{x}'(t)\underline{K}(t)\underline{x}(t) \Big|_0^T = 0. \qquad \text{(C-7)}$$

Substitution of $\underline{A}\underline{x}(t) + \underline{B}\underline{u}(t)$ for $\underline{x}(t)$ leads immediately to Eq.(C-5).

Now we will show that the control which minimizes J is given by

$$\underline{u}^*(t) = -\underline{R}^{-1}(\underline{N}' + \underline{B}'\underline{K}(t))\underline{x}(t) \qquad \text{(C-8)}$$

where $\underline{K}(t)$ satisfies the differential equation

$$\dot{\underline{K}}(t) = -\underline{K}(t)\underline{A}-\underline{A}'\underline{K}(t) + (\underline{K}(t)\underline{B}+\underline{N})\underline{R}^{-1}(\underline{N}'+\underline{B}'\underline{K}(t)) - \underline{L}$$

$$\text{(C-9)}$$

112

with terminal condition $\underline{K}(T) = \underline{Q}*$. It is clear from Eq. (C-9) that the matrix $\underline{K}(t)$, if it exists, is symmetric. The definiteness restrictions of Eq. (C-3) insure that a positive definite solution of Eq. (C-9) will exist.

If we add the identity of Eq. (C-5) to the cost functional of Eq. (C-2), we obtain

$$J = \int_0^T [\underline{x}' \quad \underline{u}'] \begin{bmatrix} \underline{L} & \underline{N} \\ \underline{N}' & \underline{R} \end{bmatrix} \begin{bmatrix} \underline{x} \\ \underline{u} \end{bmatrix} dt + \underline{x}'(T)\underline{Q}\underline{x}(t)$$

$$+ \int_0^T [\underline{x}' \quad \underline{u}'] \begin{bmatrix} \dot{\underline{K}}+\underline{K}\underline{A}+\underline{A}'\underline{K} & \underline{K}\underline{B} \\ \underline{B}'\underline{K} & \underline{0} \end{bmatrix} \begin{bmatrix} \underline{x} \\ \underline{u} \end{bmatrix} dt - \underline{x}'\underline{K}\underline{x}\bigg|_0^T . \quad (C-10)$$

Combining the two integrals and using the differential equation for $\underline{K}(t)$ yields

$$J = \int_0^T [\underline{x}' \quad \underline{u}'] \begin{bmatrix} (\underline{K}\underline{B}+\underline{N})\underline{R}^{-1}(\underline{N}'+\underline{B}'\underline{K}) & \underline{N}+\underline{K}\underline{B} \\ \underline{N}'+\underline{B}'\underline{K} & \underline{R} \end{bmatrix} \begin{bmatrix} \underline{x} \\ \underline{u} \end{bmatrix} dt$$

$$+ \underline{x}'(0)\underline{K}(0)\underline{x}(0). \quad (C-11)$$

The integral term in Eq. (C-11) is obviously non-negative as follows from Eq. (C-3). However if u(t) is chosen according to Eq. (C-8), then the integral term is identically zero and the total cost function simplifies to

---

*See note at end of Appendix.

$$J \;=\; \underline{x}(0)\underline{K}(0)\underline{x}(0). \tag{C-12}$$

Not only does the feedback gain $\underline{K}(t)$ figure in the calculation of the control, but it gives an explicit formulation for the cost of the optimal trajectory.

With the minimum cost control defined by Eq. (C-8), the optimal state trajectory is given by

$$\underline{x}(t) \;=\; \underline{A} - \underline{BR}^{-1}(\underline{N}' + \underline{B}'\underline{K}(t))\;\underline{x}(t). \tag{C-13}$$

Note that Eq. (C-9) can be rewritten as

$$\underline{\dot{K}} = -\underline{K}(\underline{A} - \underline{BR}^{-1}\underline{N}') - (\underline{A} - \underline{BR}^{-1}\underline{N}')'\underline{K} + \underline{KBR}^{-1}\underline{B}'\underline{K} - (\underline{L} - \underline{NR}^{-1}\underline{N}'),$$
$$\tag{C-14}$$

and it is easily shown that the problem defined by Eqs. (C-1) and (C-2) is equivalent to the problem

$$\min J \;=\; \underline{x}'(\underline{T})\underline{Q}\underline{x}(\underline{T}) + \int_0^T [\underline{x}' \quad \underline{u}'] \begin{bmatrix} \underline{L} - \underline{NR}^{-1}\underline{N}' & \underline{0} \\ \underline{0} & \underline{R} \end{bmatrix} \begin{bmatrix} \underline{x} \\ \underline{u} \end{bmatrix} dt$$

$$\tag{C-15}$$

subject to

$$\underline{\dot{x}}(t) \;=\; (\underline{A} - \underline{BR}^{-1}\underline{N}')\underline{x}(t) + \underline{Bu}(t). \tag{C-16}$$

This last assertion can be established by an argument paralleling that used to derive the minimum cost control of the original system.

---

*[Note: The reader should note that there has been no justification for the boundary condition $\underline{K}(T) = \underline{Q}$. This is correct, however, and can be deduced by other means including transversality conditions.]

APPENDIX D

Solution of the Algebraic Riccati Equation

Consider the linear system and quadratic cost functional

$$\underline{\dot{x}} = \underline{A}\underline{x} + \underline{B}\underline{u}; \qquad \underline{x}(0) = \underline{x}_0 \qquad \text{(D-1)}$$

$$J = \int_0^\infty [\underline{x}' \quad \underline{u}'] \begin{bmatrix} \underline{C} & \underline{0} \\ \underline{0} & \underline{R} \end{bmatrix} \begin{bmatrix} \underline{x} \\ \underline{u} \end{bmatrix} dt. \qquad \text{(D-2)}$$

We have already seen that the minimum cost control is given by

$$\underline{u}^* = -\underline{R}^{-1}\underline{B}'\underline{K}\underline{x} \qquad \text{(D-3)}$$

where $\underline{K}$ is the solution of the matrix quadratic equation

$$\underline{A}'\underline{K} + \underline{K}\underline{A} - \underline{K}\underline{B}\underline{R}^{-1}\underline{B}'\underline{K} + \underline{C} = \underline{0}. \qquad \text{(D-4)}$$

For a simplification of notation, let us define

$$\underline{D} = \underline{B}\underline{R}^{-1}\underline{B}'. \qquad \text{(D-5)}$$

If $\underline{x}$ is an n-dimensional vector, then the matrices $\underline{A}$, $\underline{C}$, $\underline{D}$, and $\underline{K}$ will be $n \times n$ dimension matrices. We will show that the solution to Eq. (D-4) can be expressed in terms of the eigenvectors of the $2n \times 2n$ matrix

$$\underline{V} = \begin{bmatrix} \underline{A}' & \underline{C} \\ \underline{D} & -\underline{A} \end{bmatrix}. \qquad \text{(D-6)}$$

Further, the poles of the closed loop minimum cost trajectory,

$$\dot{\underline{x}} = (\underline{A} - \underline{BR}^{-1} \underline{B}'\underline{K}) \underline{x} \qquad \text{(D-7)}$$

coincide with the eigenvalues of $\underline{V}$.

It will be assumed that the matrix $\underline{V}$ has a diagonal Jordan canonical form. This will be true if the eigenvalues of $\underline{V}$ are distinct, or in the case that this fails, there exist $2n$ linearly independent eigenvectors. The method to be employed can be extended to cases where $\underline{V}$ is non-diagonalizable.

We will first establish that the eigenvalues of $\underline{V}$ have quadrangular symmetry; i.e. if λ is an eigenvalue, then so are $\bar{\lambda}, -\lambda,$ and $-\bar{\lambda}$ (where the superbar denotes complex conjugate). For the matrices $\underline{A}, \underline{C},$ and $\underline{D},$ defined over the field of real numbers, it is clear that complex eigenvalues will always occur in conjugate pairs. Consider the $2n \times 2n$ matrix

$$\underline{J} = \begin{bmatrix} \underline{0} & \underline{I} \\ -\underline{I} & \underline{0} \end{bmatrix}. \qquad \text{(D-8)}$$

Notice that $\underline{J}^2 = -\underline{I}$. Thence, as is verified by direct multiplication

$$\underline{JVJ} = \underline{V}' \qquad \text{(D-9)}$$

which leads immediately to

$$-\underline{JV} = \underline{V}'\underline{J}. \qquad \text{(D-10)}$$

116

If λ is an eigenvalue of $\underline{V}$ with associate eigenvector $\underline{e}$, then from Eq. (D-10)

$$\underline{V}'\underline{J}\underline{e} \quad = \quad -\underline{J}\underline{V}\underline{e} \quad = \quad -\lambda\underline{J}\underline{e} \qquad \text{(D-11)}$$

which shows that $-\lambda$ is an eigenvalue of $\underline{V}'$ with associated eigenvector $\underline{J}\underline{e}$. But as $\underline{V}$ and $\underline{V}'$ have the same eigenvalues, we have shown that $-\lambda$ is an eigenvalue of $\underline{V}$. It can be further shown that for a well-posed system

$$\underline{\dot{x}} \quad = \quad \underline{A}\underline{x} + \underline{B}\underline{u} \; ; \qquad \underline{y} \quad = \quad \underline{F}'\underline{x} \qquad \text{(D-12)}$$

where $\underline{F}\underline{F}'=\underline{C}$, completely controllable and completely observable, no eigenvalue of $\underline{V}$ will be purely imaginary. (It should be noted that for the case of real valued eigenvalues, the quadrangular symmetry condition collapses to a simple symmetry condition; if λ is a real eigenvalue, then $-\lambda$ is also an eigenvalue.)

Thus we can take the n eigenvalues with positive real parts, $\lambda_1,\ldots,\ \lambda_n$ (the other eigenvalues are $-\lambda_1,\ldots,\ -\lambda_n$) and arrange their corresponding eigenvectors in column form $[\underline{e}_1,\ \ldots,\ \underline{e}_n]$. This $2n \times n$ matrix can be partitioned into two $n \times n$ matrices $\underline{X}$ and $\underline{Y}$ by

$$\begin{bmatrix} \underline{X} \\ \\ \underline{Y} \end{bmatrix} = \quad [\underline{e}_1,\ \ldots,\ \underline{e}_n]. \qquad \text{(D-13)}$$

Hence we can write

$$\begin{bmatrix} \underline{A}' & \underline{C} \\ \\ \underline{D} & -\underline{A} \end{bmatrix} \begin{bmatrix} \underline{X} \\ \\ \underline{Y} \end{bmatrix} = \begin{bmatrix} \underline{X} \\ \\ \underline{Y} \end{bmatrix} \underline{\Lambda} \qquad \text{(D-14)}$$

117

where $\underline{\Lambda}$ is the n × n Jordan form for the eigenvalues of $\underline{V}$ with positive real parts. The solution to Eq. (D-4) may be written

$$\underline{K} \cdot = \underline{X}\underline{Y}^{-1}. \tag{D-15}$$

The proof is quite straightforward. From Eq. (D-14) we have

$$\underline{A}'\underline{X} + \underline{C}\underline{Y} = \underline{X}\Lambda \tag{D-16}$$

$$\underline{D}\underline{X} - \underline{A}\underline{Y} = \underline{Y}\Lambda \qquad . \tag{D-17}$$

Postmultiplying Eqs. (D-16) and (D-17) by $\underline{Y}^{-1}$ (it can be shown that Y is invertible), and premultiplying Eq. (D-17) by $\underline{X}\underline{Y}^{-1}$ yields

$$\underline{A}'\underline{X}\underline{Y}^{-1} + \underline{C} = \underline{X}\Lambda\underline{Y}^{-1} \tag{D-18}$$

$$\underline{X}\underline{Y}^{-1}\underline{D}\underline{X}\underline{Y}^{-1} - \underline{X}\underline{Y}^{-1}\underline{A} = \underline{X}\Lambda\underline{Y}^{-1}. \tag{D-19}$$

Subtraction of Eq. (D-19) from Eq. (D-18) results in

$$\underline{A}'(\underline{X}\underline{Y}^{-1}) + (\underline{X}\underline{Y}^{-1})\underline{A} - (\underline{X}\underline{Y}^{-1})\underline{D}(\underline{X}\underline{Y}^{-1}) + \underline{C} = 0. \tag{D-20}$$

It can be further established that for $\underline{C}$ and $\underline{D}$ symmetric and positive semi-definite, with at least one of $\underline{C}$ or $\underline{D}$ non-singular, then $\underline{K}$ will be positive definite.

To show that the eigenvalues of $\underline{V}$ are the poles of the closed loop system, let us define the matrix $\underline{G}$ by

$$\underline{G} = \underline{Y}\Lambda\underline{Y}^{-1}. \tag{D-21}$$

Then post multiplication of Eq. (D-17) by $\underline{Y}^{-1}$ yields

$$\underline{D}\underline{K} - \underline{A} = \underline{G}. \qquad\qquad (D-22)$$

Since Eq. (D-21) represents a similarity transformation, the eigenvalues of $\underline{G}$ and $\underline{\Lambda}$ are identical; hence the eigenvalues of $\underline{A} - \underline{D}\underline{K}$, which are the poles of the closed loop minimum cost trajectory by Eq. (D-7), are given by the diagonal elements of $-\underline{\Lambda}$. Furthermore, if all the eigenvalues comprising $\underline{\Lambda}$ have positive real parts, then the system of Eq. (D-7) will be asymptotically stable.

REFERENCES

1. Bisplinghoff, R.L., Ashley, H., Halfman, R.; Aeroelasticity, Addison-Wesley, Cambridge, Mass., 1955.

2. Boeing Co.; "Boeing Model 2707 Airframe Design Report Part C: Design Criteria, Loads, Aerodynamic Heating, Flutter," Boeing Document V2-B2707-7, Sept. 1966.

3. Brockett, Roger; Finite Dimensional Linear Systems, Course Notes (Subject 6.60) M.I.T., 1969.

4. Bryson, A.E., Ho, Y.C.; Applied Optimal Control, Blaisdell, Waltham, Mass., 1969.

5. Etkin, Bernard; Dynamics of Flight, John Wiley and Sons, New York, 1959.

6. Johnson, T.L.; "The Aerodynamic Surface Location Problem in Optimal Control of Flexible Aircraft," M.I.T. E.S.L. Report - 387, 1969.

7. "LAMS: A Technology to Control Aircraft Structural Modes," 1970 Case Studies on System Control, Georgia Institute of Technology, 1970.

8. Potter, J.E.; "Matrix Quadratic Solutions," SIAM Journal of Applied Mathematics, Vol. 14, No. 3, May 1966.